Wavelet transforms and the ECG: a review

2005 Physiol. Meas. 26 R155

(http://iopscience.iop.org/0967-3334/26/5/R01)

INSTITUTE OF PHYSICS PUBLISHING PHYSIOLOGICAL MEASUREMENT

Physiol. Meas. **26** (2005) R155–R199 doi:10.1088/0967-3334/26/5/R01

TOPICAL REVIEW

Wavelet transforms and the ECG: a review

Paul S Addison

CardioDigital Ltd, Elvingston Science Centre, East Lothian, EH33 1EH, UK

E-mail: p.addison@cardiodigital.com

Received 5 April 2005, accepted for publication 30 June 2005
Published 8 August 2005
Online at stacks.iop.org/PM/26/R155

Abstract

The wavelet transform has emerged over recent years as a powerful time–frequency analysis and signal coding tool favoured for the interrogation of complex nonstationary signals. Its application to biosignal processing has been at the forefront of these developments where it has been found particularly useful in the study of these, often problematic, signals: none more so than the ECG. In this review, the emerging role of the wavelet transform in the interrogation of the ECG is discussed in detail, where both the continuous and the discrete transform are considered in turn.

Keywords: wavelet transforms, electrocardiogram

(Some figures in this article are in colour only in the electronic version)

1. Introduction

As a result of the infinite extent of the Fourier integral, analysis is time averaged. Thus it contains only globally averaged information and so has the potential to obscure transient or location specific features within the signal. This limitation can be partly overcome by introducing a sliding time window of fixed length to localize the analysis in time. This local or short time Fourier transform (STFT) provides a degree of temporal resolution by highlighting changes in spectral response with respect to time. A number of alternative time–frequency methods are now available for signal analysis. Of these, the wavelet transform has emerged over recent years as the most favoured tool by researchers for analysing problematic signals across a wide variety of areas in science, engineering and medicine (Addison 2002). It is especially valuable because of its ability to elucidate simultaneously local spectral and temporal information from a signal in a more flexible way than the STFT by employing a window of variable width. Thus wavelet transforms produce a time–frequency decomposition of the signal which separates individual signal components more effectively than the traditional short time Fourier transform (STFT). This flexible temporal–spectral aspect of the transform

allows a local scale-dependent spectral analysis of individual signal features. In this way both short duration, high frequency and longer duration, lower frequency information can be captured simultaneously. Hence the method is particularly useful for the analysis of transients, aperiodicity and other non-stationary signal features where, through the interrogation of the transform, subtle changes in signal morphology may be highlighted over the scales of interest. Another key advantage of wavelet techniques is the variety of wavelet functions available, thus allowing the most appropriate to be chosen for the signal under investigation. This is in contrast to Fourier analysis which is restricted to one feature morphology: the sinusoid. In its discrete form using orthogonal wavelet bases, the wavelet transform is particularly useful in signal coding, allowing information within the signal to be localized within a number of pertinent coefficients for compression purposes. Wavelet transform analysis has now been applied to a wide variety of biomedical signals including: the EMG, EEG, clinical sounds, respiratory patterns, blood pressure trends and DNA sequences (e.g. Dupuis and Eugene (2000), Hadjileontiadis and Panas (1997), Marrone *et al* (1999), Khalil and Duchene (2000), Petrosian *et al* (2000), Arneodo *et al* (1998)) and the subject of this review, the ECG.

This review will examine the emerging role of wavelet transform analysis in the study of the ECG. It will begin with a brief overview of the theory of the transform in its two distinct, and very different, forms—continuous and discrete. This will be followed by a detailed account of the various areas of application to the electrocardiogram, including the determination of timing intervals, the detection of abnormalities, the analysis of heart rate variability and cardiac arrhythmias and signal compression.

2. The wavelet transform

Time–frequency signal analysis methods offer simultaneous interpretation of the signal in both time and frequency which allows local, transient or intermittent components to be elucidated. Such components are often obscured due to the averaging inherent within spectral only methods, i.e. the FFT. A number of time–frequency methods are currently available for the high resolution decomposition in the time–frequency plane useful for *signal analysis*, including the short time Fourier transform (STFT), Wigner–Ville transform (WVT), Choi–Williams distribution (CWD) and the continuous wavelet transform (CWT). Of these the continuous wavelet transform has emerged as the most favoured tool by researchers as it does not contain the cross terms inherent in the WVT and CWD methods while possessing frequency-dependent windowing which allows for arbitrarily high resolution of the high frequency signal components (unlike the STFT).

Many of the ideas behind wavelet transforms have been in existence for a long time. However, wavelet transform analysis as we now know it really began in the mid 1980s where it was developed to interrogate seismic signals (Goupillaud *et al* 1984). Interest in wavelet analysis remained within a small, mainly mathematical community during the rest of the 1980s with only a handful of scientific papers coming out each year. The application of wavelet transform analysis in science and engineering really began to take off at the beginning of the 1990s, with a rapid growth in the numbers of researchers turning their attention to wavelet analysis during that decade. The last few years have each seen the publication of over 1000 refereed journal papers concerning application of the wavelet transform, and these covering all numerate disciplines.

Wavelet transforms as they are in use today come in essentially two distinct varieties or classes: the continuous wavelet transform and the discrete wavelet transform. These are now reviewed separately.

2.1. The continuous wavelet transform (CWT)

The continuous wavelet transform (CWT) is a time–frequency analysis method which differs from the more traditional short time Fourier transform (STFT) by allowing arbitrarily high localization in time of high frequency signal features. The CWT does this by having a variable window width, which is related to the scale of observation—a flexibility that allows for the isolation of the high frequency features. Another important distinction from the STFT is that the CWT is not limited to using sinusoidal analysing functions. Rather, a large selection of localized waveforms can be employed as long as they satisfy predefined mathematical criteria (described below). The wavelet transform of a continuous time signal, $x(t)$, is defined as:

$$T(a,b) = \frac{1}{\sqrt{a}} \int_{-\infty}^{+\infty} x(t)\psi^* \left(\frac{t-b}{a} \right) \mathrm{d}t \tag{1}$$

where $\psi^*(t)$ is the complex conjugate of the analysing wavelet function $\psi(t)$, a is the dilation parameter of the wavelet and b is the location parameter of the wavelet. In order to be classified as a wavelet, a function must satisfy certain mathematical criteria. These are:

(1) It must have finite energy:

$$E = \int_{-\infty}^{\infty} |\psi(t)|^2 \, \mathrm{d}t < \infty. \tag{2}$$

(2) If $\hat{\psi}(f)$ is the Fourier transform of $\psi(t)$, i.e.

$$\hat{\psi}(f) = \int_{-\infty}^{\infty} \psi(t) \, \mathrm{e}^{-\mathrm{i}(2\pi f)t} \, \mathrm{d}t \tag{3}$$

then the following condition must hold:

$$C_g = \int_0^{\infty} \frac{|\hat{\psi}(f)|^2}{f} \, \mathrm{d}f < \infty. \tag{4}$$

This implies that the wavelet has no zero-frequency component, i.e. $\hat{\psi}(0) = 0$, or to put it another way, it must have a zero mean. Equation (4) is known as the *admissibility condition* and C_g is called the *admissibility constant*. The value of C_g depends on the chosen wavelet.

(3) For complex (or analytic) wavelets, the Fourier transform must both be real and vanish for negative frequencies.

The contribution to the signal energy at the specific a scale and b location is given by the two-dimensional wavelet energy density function known as the scalogram (analogous to the *spectrogram*—the energy density surface of the STFT):

$$E(a,b) = |T(a,b)|^2. \tag{5}$$

In practice, all functions which differ from $|T(a,b)|^2$ by only a constant multiplicative factor are also called scalograms, e.g. $|T(a,b)|^2/C_g$, $|T(a,b)|^2/C_g f_c$, etc (where f_c is a characteristic frequency of the wavelet function—see later). The scalogram can be integrated across a and b to recover the total energy in the signal using the admissibility constant, C_g, as follows:

$$E = \frac{1}{C_g} \int_{-\infty}^{+\infty} \int_0^{\infty} |T(a,b)|^2 \frac{\mathrm{d}a}{a^2} \, \mathrm{d}b, \qquad \left[= \int_{-\infty}^{+\infty} x(t)^2 \, \mathrm{d}t \right]. \tag{6}$$

The relative contribution to the total energy contained within the signal at a specific a scale is given by the scale-dependent energy distribution:

$$E(a) = \frac{1}{C_g} \int_{-\infty}^{\infty} |T(a,b)|^2 \, \mathrm{d}b. \tag{7}$$

Peaks in $E(a)$ highlight the dominant energetic scales within the signal. We may convert the scale-dependent wavelet energy spectrum of the signal, $E(a)$, to a frequency-dependent wavelet energy spectrum $E_{\mathrm{W}}(f)$ in order to compare directly with the Fourier energy spectrum of the signal $E_{\mathrm{F}}(f)$. To do this, we must convert from the wavelet a scale (which can be interpreted as a representative temporal, or spatial, period for physical data) to a characteristic frequency of the wavelet such as the spectral peak frequency, passband centre, central frequency. The spectral components are inversely proportional to the dilation, i.e. $f \propto 1/a$, The frequency associated with a wavelet of arbitrary a scale is given by

$$f = \frac{f_{\mathrm{c}}}{a} \tag{8}$$

where the characteristic frequency of the mother wavelet (the archetypal wavelet at scale $a = 1$ and location $b = 0$), f_{c}, becomes a scaling constant and f is the representative or frequency for the wavelet at arbitrary scale a.

Finally, as with the Fourier transform, the original signal may be reconstructed using an inverse transform:

$$x(t) = \frac{1}{C_g} \int_{-\infty}^{\infty} \int_{0}^{\infty} T(a, b) \psi_{a,b}(t) \frac{\mathrm{d}a\, \mathrm{d}b}{a^2}. \tag{9}$$

In practice a fine discretization of the CWT is computed where usually the b location is discretized at the sampling interval and the a scale is discretized logarithmically.

As the wavelet transform given by equation (1) is a convolution of the signal with a wavelet function we can use the convolution theorem to express the integral as a product in Fourier space, i.e.,

$$T(a, b) = \frac{1}{2\pi} \int_{-\infty}^{\infty} \hat{x}(\omega) \hat{\psi}^*_{a,b}(\omega)\, \mathrm{d}\omega \tag{10a}$$

where

$$\hat{\psi}^*_{a,b}(\omega) = \sqrt{a} \hat{\psi}^*(a\omega)\, \mathrm{e}^{\mathrm{i}\omega b} \tag{10b}$$

is the Fourier spectrum of the analysing wavelet at scale a and location b. In this way, a fast Fourier transform (FFT) algorithm can be employed in practice to speed up the computation of the wavelet transform.

For its practical implementation the continuous wavelet transform is computed over a finely discretized time–frequency grid. This discretization involves an approximation of the transform integral (i.e. a summation) computed on a discrete grid of a scales and b locations. In general, the wavelet transform is approximated in this way over each time step for a range of wavelet scales; there is therefore a heavy computational burden involved in the generation of the CWT and in general an order or two in magnitude more wavelet values generated than original signal components. A vast amount of repeated information is contained within this *redundant representation* of the continuous wavelet transform $T(a, b)$. This can be condensed considerably by considering only local maxima and minima of the transform. Two definitions of these maxima are commonly used in wavelet analysis practice, these are:

(1) Wavelet *ridges*, defined as

$$\frac{\mathrm{d}(|T(a, b)^2|/a)}{\mathrm{d}a} = 0 \tag{11}$$

are used for the determination of instantaneous frequencies and amplitudes of signal components (Delprat *et al* 1992, Carmona *et al* 1997). Note that this definition of a ridge uses the rescaled scalogram, $S(a, b) = |T(a, b)|^2/a$, as it leads to a simpler analytical

solution relating the ridge locus to the instantaneous frequency when a standard Morlet wavelet is employed as the analysing wavelet. In addition, the amplitude of the ridge can be used to compute the amplitude of the instantaneous frequency component. Further, it has been shown recently how secondary wavelet transforms of ridges can be used to provide information on the frequency and amplitude modulation of the primary signal components (Addison and Watson 2004). The method, called secondary wavelet feature decoupling (SWFD), requires neither the primary signal nor the secondary modulations to be strictly stationary in nature.

(2) Wavelet *modulus maxima*, defined as

$$\frac{\mathrm{d}|T(a,b)|^2}{\mathrm{d}b} = 0 \tag{12}$$

are used for locating and characterizing singularities in the signal (Kadambe *et al* 1999, Bruce and Adhami 1999). (Note that equation (12) also includes inflection points with zero gradient. These can easily be removed when implementing the modulus maxima method in practice.)

There are many continuous wavelets to choose from; however, by far the most popular are the Mexican hat wavelet and the Morlet wavelet. These are described as follows.

2.1.1. The Mexican hat wavelet. The Mexican hat wavelet is the second derivative of a Gaussian function given by

$$\psi(t) = (1 - t^2)\,\mathrm{e}^{-\frac{t^2}{2}}. \tag{13}$$

This wavelet, shown in figure 1(b), has been used in practice for a number of data analysis tasks in science and engineering including: the morphological characterization of engineering surfaces (Lee *et al* 1998), the interrogation of laser-induced ultrasonic signals used to measure stiffness coefficients in a viscoelastic composite material (Guilbaud and Audoin 1999) and the analysis of turbulent flows (e.g. Collineau and Brunet (1993), Higuchi *et al* (1994), Addison (1999)). In addition, the Mexican hat is used extensively in studies requiring the use of modulus maxima methods as its maxima lines (and those of all other derivatives of Gaussian functions) are guaranteed continuous across scales for singularities in the signal (Mallat 1998). An example of a Mexican hat-based wavelet transform of a chirp signal is shown in figure 1(c). The increase in frequency of the components through time in the time–frequency plane is evident in the plot. Figure 2 shows the wavelet transform of an exponential discontinuity—a sudden spike in the signal half way along its length followed by a smooth exponential decay. As the transform plot has been orientated with the smallest scales at the top it 'points' to the signal discontinuity in the signal above.

A complex version of the Mexican hat function can easily be constructed by simply setting the negative part of its Fourier frequency spectrum to zero before performing an inverse Fourier transform to get the analytic version of the Mexican hat shown (Addison *et al* 2002b). However, in practice the Morlet wavelet is used when a complex wavelet function is required. Note that the Mexican hat normally used in practice (i.e. that given by equation (13) and shown in figure 1(b)) is actually the negative of the second derivative of the Gaussian function. All derivatives of the Gaussian function may be employed as a wavelet. Which is the most appropriate one to use depends on the application. The first and second derivatives of the Gaussian are shown in figures 1(a) and (b), respectively. These are the two that are most often used in practice. Higher order derivatives are less commonplace.

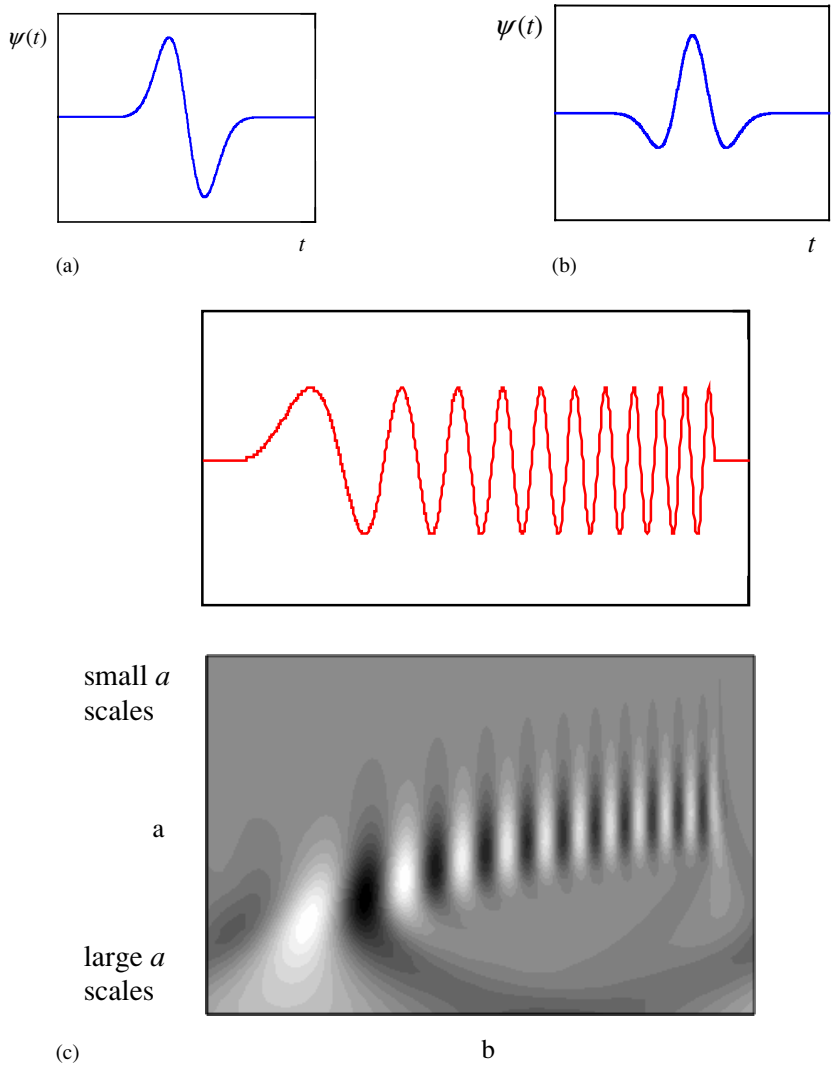

Figure 1. Segment of a chirp signal with associated transform plot: (a) Gaussian wave (first derivative of a Gaussian), (b) Mexican hat (second derivative of a Gaussian). (c) Mexican hat-based transform of chirp signal (small/large a scales correspond to high/low frequency components respectively). (Reprinted from Addison 2002 *The Illustrated Wavelet Transform Handbook* chapter 2. With kind permission of the Institute of Physics Publishing.)

2.1.2. The Morlet wavelet. The Morlet wavelet is the most popular complex wavelet used in practice. The complete Morlet wavelet is defined as

$$\psi(t) = \frac{1}{\sqrt[4]{\pi}}\left(e^{i\omega_o t} - e^{-\frac{\omega_o^2}{2}}\right) e^{-\frac{t^2}{2}} \tag{14}$$

where ω_o is the central frequency of the mother wavelet. The second term in the brackets is known as the correction term, as it corrects for the non-zero mean of the complex sinusoid of the first term. In practice it becomes negligible for values of $\omega_o > 5$. Previous investigators have concentrated on wavelet transforms with ω_o in the range 5–6, where it can be performed

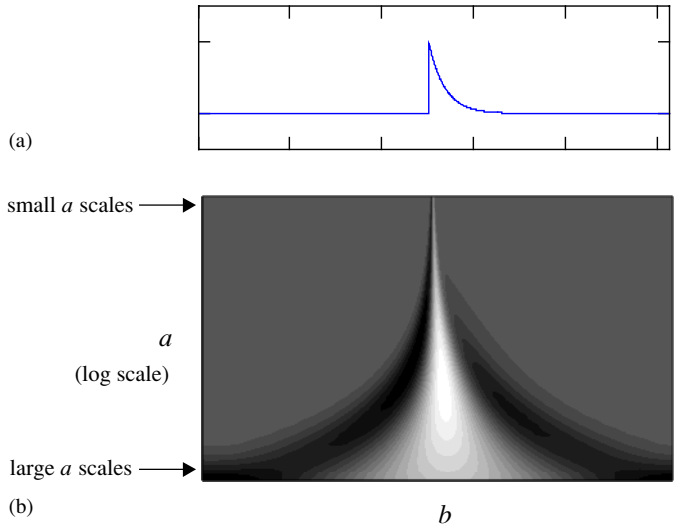

Figure 2. Pointing to an exponential discontinuity. (a) A sudden spike with an exponential tail. (b) The transform plot for the discontinuity. (Reprinted from Addison 2002 *The Illustrated Wavelet Transform Handbook* chapter 2. With kind permission of the Institute of Physics Publishing.)

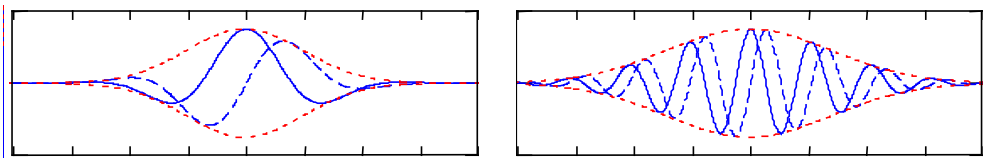

Figure 3. Two Morlet wavelets: left $\omega_o = 2.0$ ($f_o = 0.318$) and right $\omega_o = 12$ ($f_o = 1.909$).

without the correction term since it becomes very small. In this case, the Morlet wavelet becomes

$$\psi(t) = \frac{1}{\sqrt[4]{\pi}} e^{i\omega_o t} e^{-\frac{t^2}{2}}. \tag{15}$$

This truncated Morlet wavelet is almost invariably used in the literature and often referred to as simply the *Morlet wavelet*. In this paper we use the name *standard Morlet wavelet* for this simplified form and *complete Morlet wavelet* for the complete form given by equation (14). However, it has been shown that lowering of ω_o below 5 allows an interrogation that is 'more temporal than spectral' which can be useful for some data analysis tasks (Addison *et al* 2002b). Two examples of Morlet wavelets are shown in figure 3.

Figure 4 contains the same chirp signal as that shown above in figure 1. The Morlet wavelet with $\omega_o = 5.33$ rad s^{-1} (i.e. $f_0 = 0.849$ Hz) was used to transform the signal. The real part of the transformed signal is plotted in figure 4(b) and has similarities with the Mexican hat transform plot in figure 1(c). The discontinuities at the beginning and end of the chirp segment are picked up well in the phase plot of figure 4(c). These are located using arrows at the top of the phase plot. The continuous increase in instantaneous frequency associated with the chirp is highlighted in the modulus plot of figure 4(d). The instantaneous frequency associated with a signal component can be found from its wavelet transform ridges. These are the maxima found in the rescaled wavelet transform scalogram. The ridge associated with the

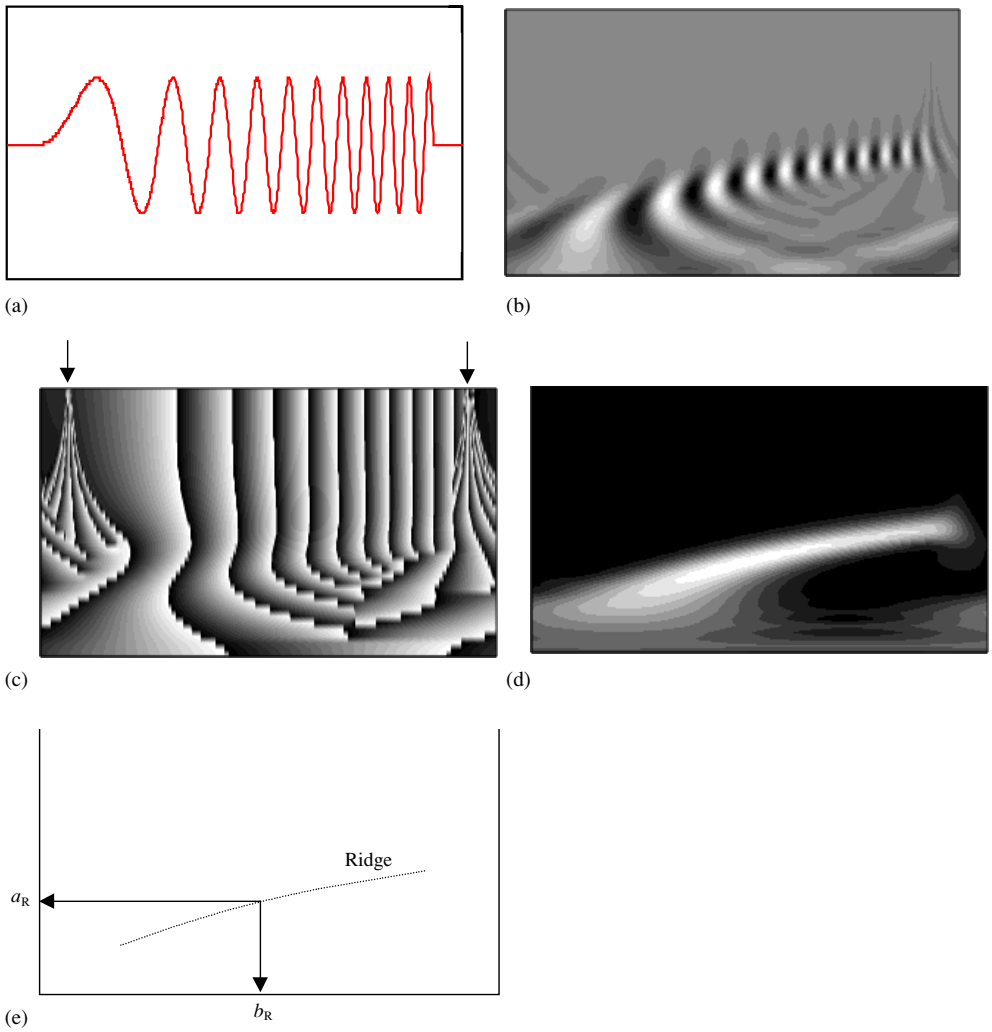

Figure 4. Segment of a chirp signal with associated transform plots—Morlet wavelet. (a) Chirp signal segment, (b) real part of Morlet wavelet transform, (c) phase, (d) modulus and (e) a schematic of the ridge found from the maxima of the rescaled scalogram $\frac{|T(a,b)|^2}{a}$. The instantaneous frequency at time b_R can be found from a_R. We can see the relation between maxima in the rescaled scalogram and instantaneous frequency by substituting a complex sinusoid as the signal $x(t)$ in the wavelet transform integral given by equation (1), and using a Morlet wavelet. Then, using a change of variable $t' = (t - b)/a$, it can be shown that maxima in the rescaled scalogram correspond to the instantaneous frequencies through their associated scales. (Reprinted from Addison 2002 The Illustrated Wavelet Transform Handbook chapter 2. With kind permission of the Institute of Physics Publishing.)

chirp signal is shown schematically in figure 4(e), where the instantaneous scale a_R at time b_R can be used to find the instantaneous frequency f_R ($= f_0/a_R$). The instantaneous amplitude and phase can also be found from the ridge. Further, if we plot the rescaled scalogram in terms of a characteristic wavelet frequency where $f = f_0/a$, then the instantaneous frequency can be read directly off this plot.

The standard Morlet wavelet has a form very similar to the analysing function used for the short time Fourier transform employing a Gaussian window (sometimes called a Gabor

transform). The important difference is that, for the Morlet wavelet transform, the window and enclosed sinusoid are scaled together, whereas for the STFT we keep the window length constant and scale only the enclosed sinusoid. The wavelet can therefore localize itself in time for short duration, i.e. high frequency, fluctuations. There is, however, an associated spreading of the frequency distribution associated with wavelets of short duration. Conversely, there is a spreading in temporal resolution at low frequencies. This is highlighted for an ECG signal at the beginning of section 3.

2.2. The discrete wavelet transform (DWT)

In its most common form, the DWT employs a dyadic grid (integer power of two scaling in a and b) and orthonormal wavelet basis functions and exhibits zero redundancy. (Actually, the transform integral remains continuous for the DWT but is determined only on a discretized grid of a scales and b locations. In practice, the input signal is treated as an initial wavelet approximation to the underlying continuous signal from which, using a multiresolution algorithm, the wavelet transform and inverse transform can be computed discretely, quickly and without loss of signal information.) A natural way to sample the parameters a and b is to use a logarithmic discretization of the a scale and link this, in turn, to the size of steps taken between b locations. To link b to a we move in discrete steps to each location b, which are proportional to the a scale. This kind of discretization of the wavelet has the form

$$\psi_{m,n}(t) = \frac{1}{\sqrt{a_0^m}}\psi\left(\frac{t - nb_0a_0^m}{a_0^m}\right) \tag{16}$$

where the integers m and n control the wavelet dilation and translation respectively; a_0 is a specified fixed dilation step parameter set at a value greater than 1, and b_0 is the location parameter which must be greater than zero. A common choice for discrete wavelet parameters a_0 and b_0 are 2 and 1 respectively. This power-of-two logarithmic scaling of both the dilation and translation steps is known as the dyadic grid arrangement. The *dyadic grid* is perhaps the simplest and most efficient discretization for practical purposes and lends itself to the construction of an orthonormal wavelet basis. Substituting $a_0 = 2$ and $b_0 = 1$ into equation (16) we see that the dyadic grid wavelet can be written compactly, as

$$\psi_{m,n}(t) = 2^{-m/2}\psi(2^{-m}t - n). \tag{17}$$

Note that this has the same notation as the general discrete wavelet given by equation (16). From here on, $\psi_{m,n}(t)$ will be used only to denote dyadic grid scaling with $a_0 = 2$ and $b_0 = 1$. Discrete dyadic grid wavelets are usually chosen to be orthonormal, i.e. they are both orthogonal to each other and are normalized to have unit energy. This is expressed as

$$\int_{-\infty}^{\infty} \psi_{m,n}(t)\psi_{m',n'}(t)\,\mathrm{d}t = \begin{cases} 1 & \text{if} \quad m = m' \text{ and } n = n' \\ 0 & \text{otherwise.} \end{cases} \tag{18}$$

This means that the information stored in a wavelet coefficient $T_{m,n}$ obtained from the wavelet transform is not repeated elsewhere and allows for the complete regeneration of the original signal without redundancy. The corresponding family of orthonormal wavelets is an orthonormal basis. (A basis is a set of vectors, a combination of which can completely define the signal, $x(t)$. An orthonormal basis has component vectors which, in addition to being able to completely define the signal, are perpendicular to each other.) Figure 5 shows a number of examples of orthonormal wavelets.

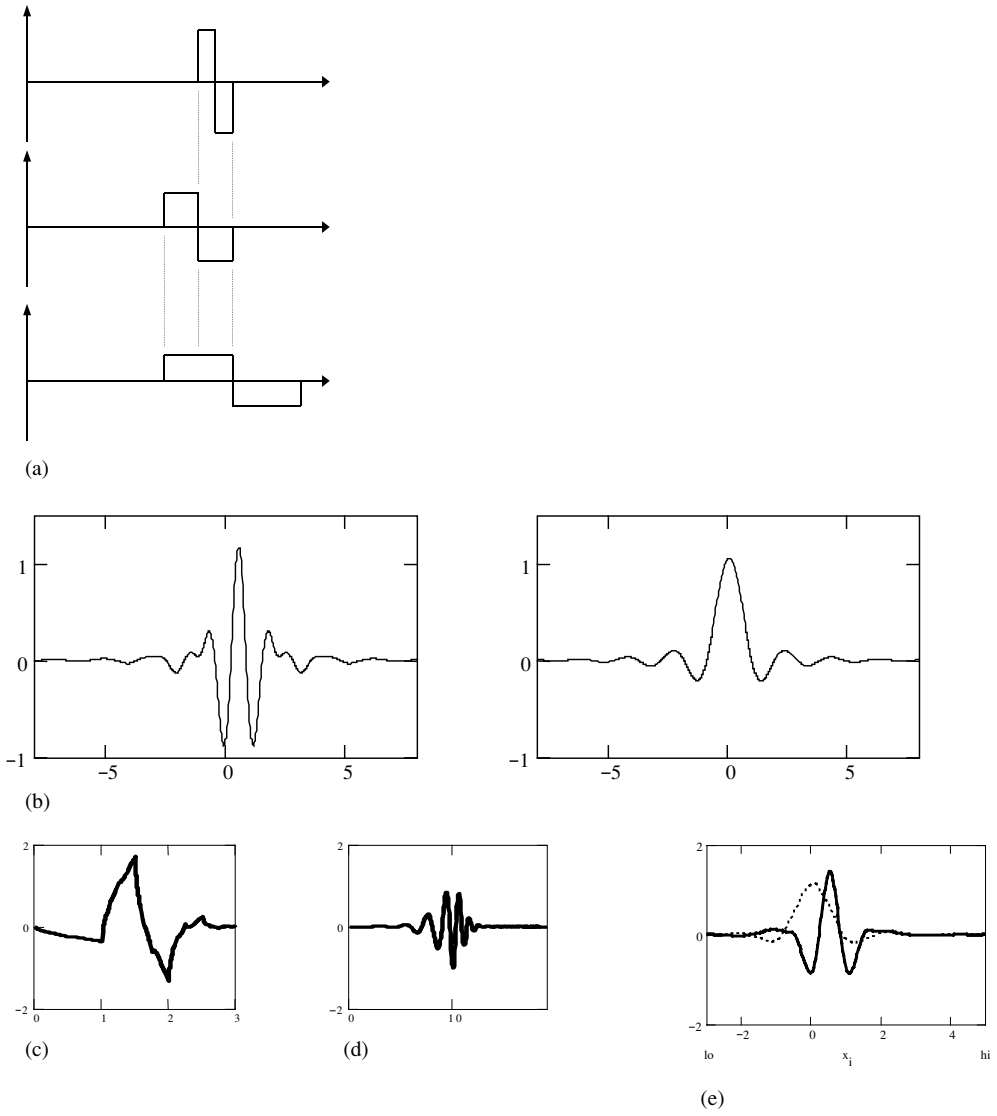

Figure 5. Examples of discrete orthogonal wavelets. (a) Three Haar wavelets at three consecutive scales on a dyadic grid. (b) A Meyer wavelet and associated scaling function (right). (c) Daubechies D4 wavelet. (d) Daubechies D20 wavelet. (e) C18 Coiflet wavelet (scaling function shown dotted).

Using the dyadic grid wavelet of equation (17), the *discrete wavelet transform* (DWT) can be written as:

$$T_{m,n} = \int_{-\infty}^{\infty} x(t)\psi_{m,n}(t)\,\mathrm{d}t \tag{19}$$

where $T_{m,n}$ is known as the wavelet (or detail) coefficient at scale and location indices (m, n).

Before continuing it is important to make clear the distinct difference between the DWT and the discretized approximations of the CWT used in practice. The discretizations of the continuous wavelet transform, required for its practical implementation, involve a discrete approximation of the transform integral (i.e. a summation) computed on a discrete grid of

a scales and b locations. The inverse continuous wavelet transform is also computed as a discrete approximation. How close an approximation to the original signal is recovered depends mainly on the resolution of the discretization used and, with care, usually a very good approximation can be recovered. On the other hand, for the DWT, as defined in equation (19), the transform integral remains continuous but is determined only on a discretized grid of a scales and b locations. We can then sum the DWT coefficients to infinity over m and n to get the original signal back exactly. We will see later in this section how, given an initial discrete input signal, which we treat as an initial approximation to the underlying continuous signal, we can compute the wavelet transform and inverse transform discretely, quickly and without loss of signal information.

Orthonormal dyadic discrete wavelets are associated with *scaling functions* and their dilation equations. The scaling function is associated with the smoothing of the signal and has the same form as the wavelet, given by

$$\phi_{m,n}(t) = 2^{-m/2}\phi(2^{-m}t - n). \tag{20}$$

They have the property

$$\int_{-\infty}^{\infty} \phi_{0,0}(t)\,\mathrm{d}t = 1 \tag{21}$$

where $\phi_{0,0}(t) = \phi(t)$ is sometimes referred to as the father scaling function or father wavelet (cf mother wavelet). (The integral of a wavelet function is zero.) The scaling function is orthogonal to translations of itself, *but not to dilations of itself*. The scaling function can be convolved with the signal to produce *approximation coefficients* as follows

$$S_{m,n} = \int_{-\infty}^{\infty} x(t)\phi_{m,n}(t)\,\mathrm{d}t. \tag{22}$$

From the above, we can see that the approximation coefficients are simply weighted averages of the continuous signal factored by $2^{m/2}$. The approximation coefficients at a specific scale m are collectively known as the *discrete approximation* of the signal at that scale. A *continuous approximation* of the signal at scale m can be generated by summing a sequence of scaling functions at this scale factored by the approximation coefficients as follows

$$x_m(t) = \sum_{n=-\infty}^{\infty} S_{m,n}\phi_{m,n}(t) \tag{23}$$

where $x_m(t)$ is a smooth, scaling-function-dependent version of the signal $x(t)$ at scale index m. This continuous approximation approaches $x(t)$ at small scales, i.e. as $m \to -\infty$. A signal $x(t)$ can then be represented using a combined series expansion using both the approximation coefficients and the wavelet (detail) coefficients as follows

$$x(t) = \sum_{n=-\infty}^{\infty} S_{m_0,n}\phi_{m_0,n}(t) + \sum_{m=-\infty}^{m_0}\sum_{n=-\infty}^{\infty} T_{m,n}\psi_{m,n}(t). \tag{24}$$

We can see from this equation that the original continuous signal is expressed as a combination of an approximation of itself, at arbitrary scale index m_0, added to a succession of signal details from scales m_0 down to negative infinity. The *signal detail* at scale m is defined as

$$d_m(t) = \sum_{n=-\infty}^{\infty} T_{m,n}\psi_{m,n}(t) \tag{25}$$

hence we can write equation (24) as

$$x(t) = x_{m_0}(t) + \sum_{m=-\infty}^{m_0} d_m(t). \tag{26}$$

From this equation it is easy to show that

$$x_{m-1}(t) = x_m(t) + d_m(t) \tag{27}$$

which tells us that if we add the signal detail at an arbitrary scale (index m) to the approximation at that scale we get the signal approximation at an increased resolution (i.e. at a smaller scale, index $m-1$). This is called a *multiresolution representation* (Mallat 1989).

2.2.1. Coefficients from coefficients: multiresolution and the fast wavelet transform. The approximation coefficients at scale index $m+1$ can be generated using the scaling coefficients at the previous scale.

$$S_{m+1,n} = \frac{1}{\sqrt{2}} \sum_k c_k S_{m,2n+k} = \frac{1}{\sqrt{2}} \sum_k c_{k-2n} S_{m,k}. \tag{28}$$

Similarly the wavelet coefficients can be found from the approximation coefficients at the previous scale using the reordered scaling coefficients b_k as follows

$$T_{m+1,n} = \frac{1}{\sqrt{2}} \sum_k b_k S_{m,2n+k} = \frac{1}{\sqrt{2}} \sum_k b_{k-2n} S_{m,k}. \tag{29}$$

We can see now that if we know the approximation coefficients $S_{m_0,n}$ at a specific scale m_0 then, through the repeated application of equations (28) and (29), we can generate the approximation and detail wavelet coefficients at all scales larger than m_0. Note that, to do this, we do not even need to know exactly what the underlying continuous signal $x(t)$ is, only $S_{m_0,n}$. Equations (28) and (29) represent the multiresolution *decomposition algorithm*. The decomposition algorithm is the first half of the *fast wavelet transform* which allows us to compute the wavelet coefficients in this way, rather than computing them laboriously from the convolution of equation (19). Iterating equations (28) and (29) performs, respectively, a highpass and lowpass filtering of the input (i.e. the coefficients $S_{m,2n+k}$) to get the outputs ($S_{m+1,n}$ and $T_{m+1,n}$). The vectors containing the sequences $\frac{1}{\sqrt{2}}c_k$ and $\frac{1}{\sqrt{2}}b_k$ represent the filters: $\frac{1}{\sqrt{2}}c_k$ is the *lowpass filter*, letting through low signal frequencies and hence a smoothed version of the signal, and $\frac{1}{\sqrt{2}}b_k$ is the *highpass filter*, letting through the high frequencies corresponding to the signal details. The filter coefficients determine the wavelet used. The reader is referred to Daubechies (1992) for more information on coefficients (including listings) and the resulting properties of their associated wavelets.

We can go in the opposite direction and reconstruct $S_{m,n}$ from $S_{m+1,n}$ and $T_{m+1,n}$ using the *reconstruction algorithm*:

$$S_{m-1,n} = \frac{1}{\sqrt{2}} \sum_k c_{n-2k} S_{m,k} + \frac{1}{\sqrt{2}} \sum_k b_{n-2k} T_{m,k} \tag{30}$$

where we have reused k as the location index of the transform coefficients at scale index m to differentiate it from n, the location index at scale $m-1$. Hence, at the smaller scale, $m-1$, the approximation coefficients can be found in terms of a combination of approximation and detail coefficients at the next scale, m. Note that if there are only a finite number of non-zero scaling coefficients ($=N_K$), then c_{n-2k} has non-zero values only when in the range 0 to $N_k - 1$. The reconstruction algorithm is the second half of the multiresolution algorithm.

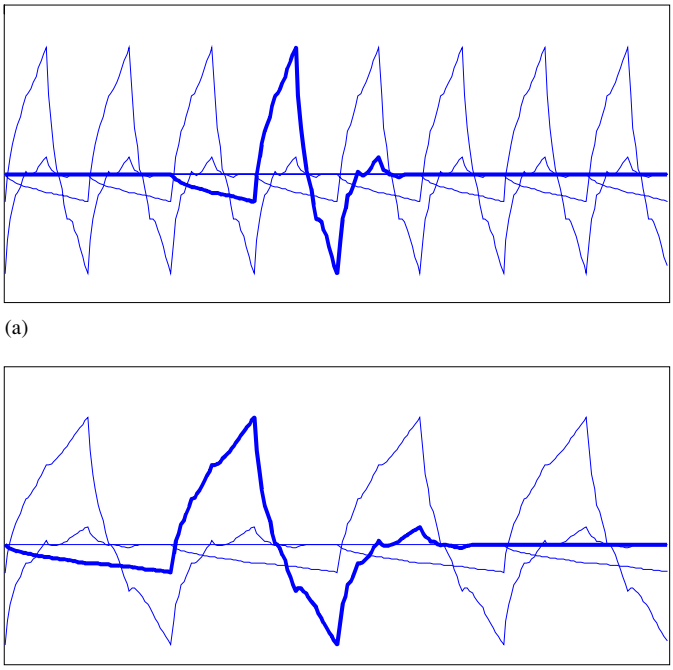

Figure 6. Covering the time axis with dyadic grid wavelets. (a) Eight Daubechies D4 wavelets covering the time axis at scale m. (b) Four Daubechies D4 wavelets covering the time axis at scale $m + 1$. These wavelets are twice the width of those in (a). (Reprinted from Addison 2002 *The Illustrated Wavelet Transform Handbook* chapter 3. With kind permission of the Institute of Physics Publishing.)

2.2.2. Discrete input signals of finite length. In practice, discrete input signals are analysed. This is generally taken to be the signal approximation coefficients at scale index $m = 0$. (Although this is not correct: see Strang and Nguyen (1996) for further discussion concerning this practice.) In addition, this series of coefficients, $S_{0,n}$, is of finite length N, which is an integer power of 2: $N = 2^M$. Thus the range of scales that can be investigated is $0 < m < M$. Substituting both $m = 0$ and $m = M$ into equation (24), and noting that we have a finite range of n which halves at each scale, we can see that the signal approximation scale $m = 0$ (the input signal) can be written as the smooth signal at scale M plus a combination of detailed signals as follows

$$\sum_{n=0}^{2^{M-m}-1} S_{0,n}\phi_{0,n}(t) = S_{M,n}\phi_{M,n}(t) + \sum_{m=1}^{M}\sum_{n=0}^{2^{M-m}-1} T_{m,n}\psi_{m,n}(t). \tag{31}$$

This is the form used to describe our finite length discrete signal in terms of its discrete wavelet expansion. The covering of a finite length time segment with wavelets is illustrated in figure 6 for Daubechies D4 wavelets at two successive scales. The lower scale covers the time window using eight wavelets, and the larger scale uses four wavelets. One of the wavelets in each plot is shown bold for clarity. The wavelets shown which spill over the end of the window have been wrapped around back to the beginning. Known as *wraparound*, it is the simplest and one of the most common treatments of the boundary for a finite length signal. However, note that by employing this method, we assume that the signal segment under investigation

represents one period of a periodic signal and we are in effect pasting the end of the signal back onto the beginning. Obviously, if the signal is not periodic, and in practice it usually is not, then we create artificial singularities at the boundary which results in large detail coefficients generated near to the boundary: a point very often overlooked in practice. Details of other methods for treating the boundaries can be found in Addison (2002).

We can rewrite equation (31) as

$$x_0(t) = x_M(t) + \sum_{m=1}^{M} d_m(t) \tag{32}$$

where the mean signal approximation at scale M is

$$x_M(t) = S_{M,n}\phi_{M,n}(t). \tag{33}$$

As the approximation coefficients are simply factored, weighted averages of the signal then, when wraparound is employed to deal with the boundaries, the single approximation component $S_{M,n}$ is related to the mean of the input signal through the relationship $\overline{S_{0,n}} = S_{M,n}/\sqrt{2^M}$ where the overbar denotes the mean of the sequence $S_{0,n}$. In addition, when wraparound has been used to deal with the boundaries, the mean signal approximation at the largest scale, $x_M(t)$, is a constant valued function equal to the input signal mean.

After a full decomposition, the energy contained within the coefficients at each scale is given by

$$E_m = \sum_{n=0}^{2^{M-m}-1} (T_{m,n})^2. \tag{34}$$

A wavelet based power spectrum of the signal may be produced using these scale-dependent energies. To do so, we require a frequency measure which is a reciprocal of the wavelet dilation e.g. the passband centre of the power spectrum of the wavelet. A wavelet power spectrum can then be produced for the signal which is directly comparable with both its Fourier and continuous wavelet counterparts. The sum of the energies contained in the detail and approximation coefficients is equal to the energy in the discrete input signal, and this is true for the energy at all stages of the multiresolution decomposition.

The term on the far right of equation (32) represents the series expansion of the fluctuating components of the finite length signal at various scales in terms of its detail coefficients. The detail signal approximation corresponding to scale index m is defined for a finite length signal as

$$d_m(t) = \sum_{n=0}^{2^{M-m}-1} T_{m,n}\psi_{m,n}(t). \tag{35}$$

As we saw above (equation (32)), adding the approximation of the signal at scale index M to the sum of all detail signal components across scales $0 < m < M$ gives the approximation of the original signal at scale index 0. Figure 7 shows the details of a chirp signal with a short burst of noise added to the middle of it. A Daubechies D20 wavelet was used in the decomposition. The original signal is shown at the top of the plot. Below the signal the details for ten wavelet scales, $d_1(t)$ to $d_{10}(t)$, are shown. The bottom trace is the remaining signal approximation $x_{10}(t)$. Adding together all these details plus the remaining approximation (which is the signal mean) returns the original signal. Two things are noticeable from the plot. First, there is a shift to the left of the large amplitude details with increasing scale, as we would expect as the chirp oscillation increases in frequency from left to right. The second thing to notice is that the high frequency burst of noise is captured at the smallest scales, again as we would expect.

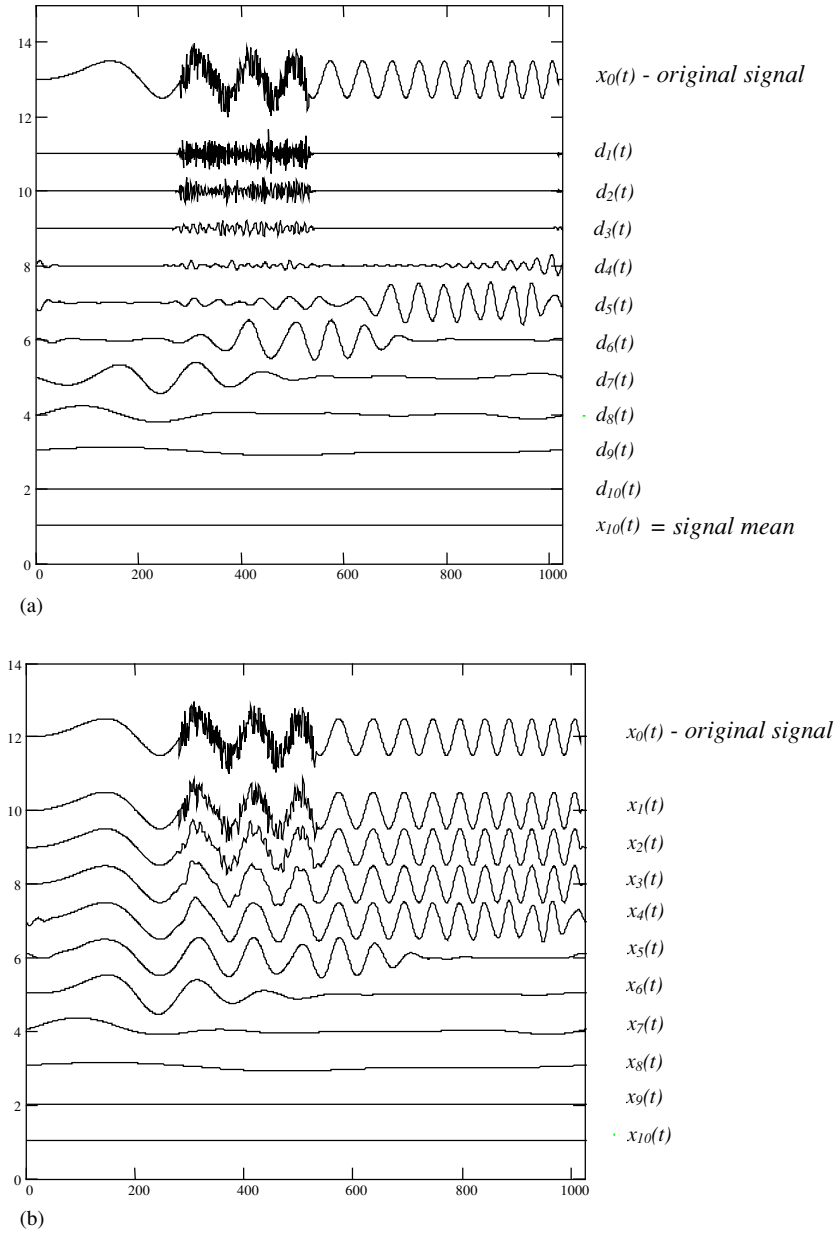

Figure 7. Multiresolution decomposition of a chirp signal containing a short burst of noise. (a) Signal details $d_m(t)$. (The signals have been displaced from each other on the vertical axis to aid clarity.) (b) Signal approximations $x_m(t)$. (Reprinted from Addison 2002 *The Illustrated Wavelet Transform Handbook* chapter 3. With kind permission of the Institute of Physics Publishing.)

Figure 8 contains an example of a wavelet decomposition of a test signal using a discrete wavelet. The input signal is composed of a section of a sine wave, some high frequency noise and a flatline. The signal is decomposed using a Daubechies D6 wavelet. A member of this family is shown in figure 8(b). The discrete transform plot is shown in figure 8(c) where the

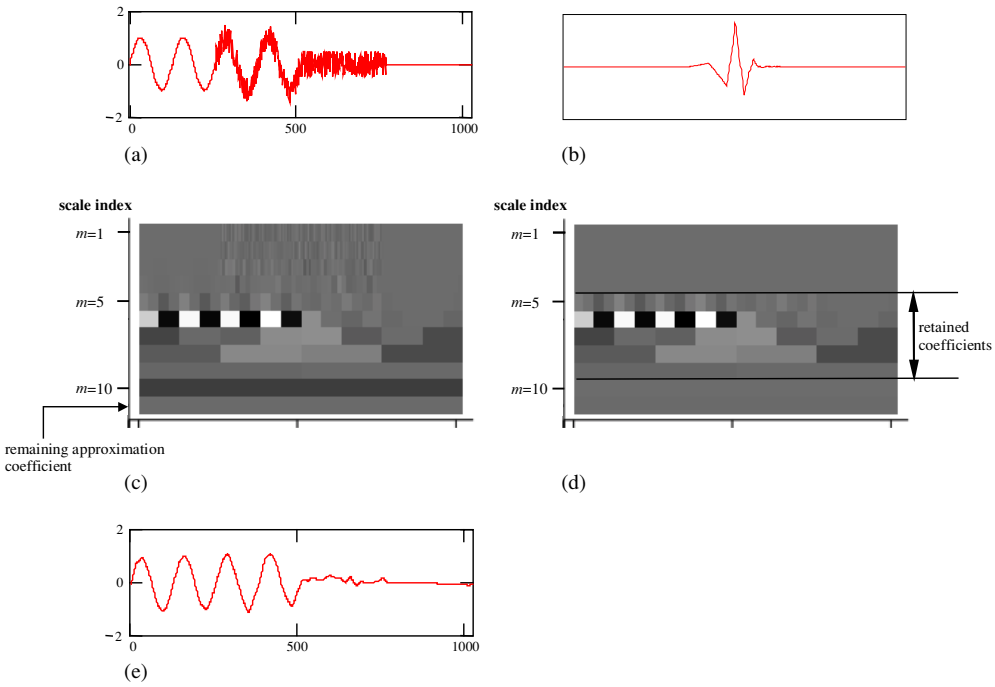

Figure 8. Discrete wavelet transform of a composite signal. The original composite signal (a) is composed of three segments: a sinusoid, uniformly distributed noise and a flatline. The signal is decomposed using Daubechies D6 wavelets (b) to give the dyadic array of transform coefficients plotted in (c). The coefficients corresponding to scales 5 to 9 are kept (d) and used to reconstruct the signal in (e). Note that a grey scale is used to depict the coefficient values, where the maximum value is white and the minimum value is black. (a) Original composite signal. (b) A member of the Daubechies D6 wavelet family. (c) Discrete transform plot. (Note dyadic structure—large positive coefficient values are white and large negative values black.) (d) Coefficient removal. (e) Reconstructed signal using only retained coefficients in (d). (Reprinted from Addison 2002 *The Illustrated Wavelet Transform Handbook* chapter 3. With kind permission of the Institute of Physics Publishing.)

dyadic grid arrangement may be seen clearly. This plot is simply a discretized dyadic map of the detail coefficients, $T_{m,n}$, where the coefficients at larger scales have correspondingly longer boxes (as the wavelets cover larger segments of the input signal). In addition to the detail coefficients, $T_{m,n}$, the remaining approximation coefficient $S_{M,0}$ is added to the bottom of the plot. As we would expect it covers the whole time axis. We can see from the transform plot that the dominant oscillation is picked up at scale index $m = 6$ and the high frequency noise is picked up within the middle segment of the transform plot at the smaller scales. We can use the reconstruction algorithm (equation (30)) to get back the original input signal $S_{0,n}$ from the array of detail coefficients shown in figure 8(c). Alternatively, we can reconstruct a modified version of the input signal by using only selected coefficients in the reconstruction. This is shown in figures 8(d) and (e) where only the coefficients corresponding to scales $m = 5$ to 8 are kept (the others are set to zero) and the signal is reconstructed. This has removed a significant amount of the noise from the signal although the sinusoidal waveform is less smooth than the original in figure 8(a). There are many more sophisticated methods to remove noise which retain the most significant signal coefficients before reconstructing. A number of thresholding methods have been developed to allow the optimum selection of

the most pertinent components. (A full treatment of wavelet thresholding methods is outwith the scope of this text. The reader is referred instead to Abramovich *et al* (2000) for a concise summary of the commonly used wavelet thresholding methods together with a comprehensive list of references on the subject.) Data compression methods require that only those wavelet coefficients which carry most of the signal information are identified and retained for use in the reconstruction of the signal. Thresholding methods have also been used to determine the significant coefficients pertaining to a pertinent signal feature, e.g. for ECG analysis they can be used to determine the location of the QRS peak.

We have glossed over much of the mathematical detail of multiresolution analysis here. Most mathematical accounts of the subject begin with a discussion of orthogonal nested subspaces and the signal approximations and details, $x_m(t)$ and $d_m(t)$, as projections onto these spaces. This more mathematical tack has not been followed herein, see for example Mallat (1998), Blatter (1998), Sarkar and Su (1998) or Williams and Armatunga (1994).

2.2.3. Methods derivative of the DWT. The discrete wavelet transform has emerged as a particularly powerful tool for the encoding of data required for compression systems. Wavelet packet transforms (WPTs) are a generalization of the discrete wavelet transform which involve particular linear combinations of discrete wavelets and the decomposition of a signal is performed in a manner similar to the multiresolution algorithm given earlier for the discrete wavelet transform. The difference being that, in the WPT signal decomposition, both the approximation and detailed coefficients are further decomposed at each level. At each stage in the decomposition, the wavelet packet algorithm partitions the time–frequency plane into rectangles of constant aspect ratio. The optimal WPT coefficient selection is chosen to represent the signal based on some predefined criterion. This criterion is normally based on an information cost function which aims to retain as much information in as few coefficients as possible. The most common measure of information used is the Shannon entropy measure (Addison 2002). Low entropies occur when the larger coefficient energies are concentrated at only a few discrete locations. In practice, the set of N wavelet packet coefficients which contain the least entropy are selected to represent the signal. That is, we want as much of the signal information to be concentrated within as few coefficients as possible. To find these coefficients the WPT coefficients are inspected and at each scale, each pair of partitioned coefficients sets are compared to those from which they were derived. Once the whole WP array has been inspected and the minimum entropy criterion employed, an optimal tiling of the time–frequency plane (with respect to the localization of coefficient energies) is obtained. This tiling provides the best basis for the signal decomposition.

Both the DWT and WPT lack translation invariance. Translation invariance simply means that if you shift the analysis along the signal by an arbitrary amount all your transform coefficients simply move along by the same amount. For the dyadic grid structure of the discrete wavelet transform this is clearly not the case: only if you shift along by the grid spacing at that scale do the coefficients become translation invariant at that scale and below. For the discretization of the continuous wavelet transform used in practice, the transform values are translation invariant only if shifted by any integer multiple of the discrete time steps, i.e. it is effectively translation invariant as the minimum shift would be the sampling interval of the signal. The stationary wavelet transform (SWT) is an offshoot of the DWT whereby the scales are dyadic but the time steps are not subsampled at each level and hence are not dyadic. This destroys orthogonality in the transform and also leads to the generation of many more coefficients, but does provide translation invariance. Although orthogonality is destroyed, the SWT is very useful for some statistical applications (Coifman and Donoho 1995). The SWT is also known by a variety of names in the literature including the dyadic

wavelet transform (i.e. dyadic in scales), maximal overlap transform and the redundant wavelet transform. It is outwith the scope of this paper to consider the wavelet packet transform and the stationary wavelet transform in more detail. For more information concerning the theory of these derivatives of the DWT the reader is referred to chapter 3 of Addison (2002).

3. Application of wavelet analysis to the electrocardiogram

Muscular contraction is associated with electrical changes known as depolarization. The electrocardiogram (ECG) is a measure of this electrical activity associated with the heart. The ECG is measured at the body surface and results from electrical changes associated with activation first of the two small heart chambers, the atria, and then of the two larger heart chambers, the ventricles. The contraction of the atria manifests itself as the 'P' wave in the ECG and contraction of the ventricles produces the feature known as the 'QRS' complex. The subsequent return of the ventricular mass to a rest state—repolarization— produces the 'T' wave. Repolarization of the atria is, however, hidden within the dominant QRS complex. Analysis of the local morphology of the ECG signal and its time varying properties has produced a variety of clinical diagnostic tools. In this section we review the application of the wavelet transform to the analysis of the ECG signal.

Figure 9 illustrates the shortcomings of traditional short term Fourier transform (STFT) analysis in detecting signal features of short duration. The figure contains a scalogram and a spectrogram corresponding to the rhythmic ECG signal shown at the top of the figure. (The signal is actually derived from a pig heart which has been shocked several times.) The spectrogram is generated from an STFT employing a 3.4 s Hanning window—typical for the analysis of this type of signal. The smearing and hence loss of local information across the spectrogram over these time scales is evident in the plot. Figure 10 contains three beats of a sinus rhythm from a human heart together with its (Morlet) wavelet energy scalogram shown as both a plan view (figure 10(b)) and a three-dimensional surface relief (figure 10(c)). Note that the logarithm of the energy is plotted in the figures as it allows for features with large differences in their energy to be made visible in the same plot. The QRS complex of the waveform manifests itself as the conical structures in figure 10(b). These converge to the high frequency components of the R spike. The P and T waves are also labelled in the plot. In addition, the continuous band evident in the plot at a frequency of around 2 Hz corresponds to the beat frequency of the sinus rhythm. The 3D morphology of the signal in wavelet space is shown in figure 10(c). Figures 9 and 10 highlight the ability to separate out signal components through the wavelet decomposition.

3.1. ECG timing, morphology, distortions and noise

Producing an algorithm for the detection of the P wave, QRS complex and T wave in an ECG is a difficult problem due to the time varying morphology of the signal subject to physiological conditions and the presence of noise. Recently, a number of wavelet-based techniques have been proposed to detect these features. Senhadji *et al* (1995) compared the ability of three different wavelets transforms (Daubechies, spline and Morlet) to recognize and describe isolated cardiac beats. Sahambi *et al* (1997a, 1997b) employed a first-order derivative of the Gaussian function as the wavelet for the characterization of ECG waveforms. They then used modulus maxima-based wavelet analysis employing the dyadic wavelet transform to detect and measure various parts of the signal, specifically the location of the onset and offset of the QRS complex and P and T waves. Sahambi *et al* showed that the algorithm performed well in the presence of modelled baseline drift and high frequency noise added to the signal. They used the method to determine timing intervals of the ECG signal including the widths of the QRS

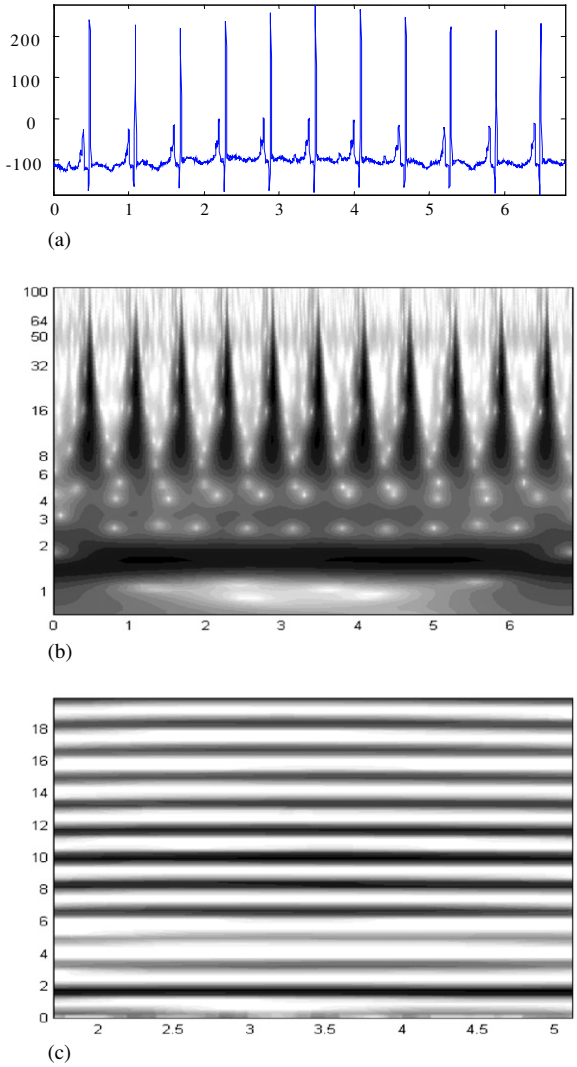

Figure 9. Wavelet scalogram versus STFT spectrogram for rhythmic signal. (a) Original rhythmic ECG signal. (b) Morlet based scalogram corresponding to (a). (c) Spectogram corresponding to (a) generated using a short time Fourier transform with a 3.4 s Hanning window.

complex, T and P waves, and PR, ST and QT intervals. The measurements of these intervals give the relative position of the components in the ECG which are important in delineating the electrical activity of the heart. Improvements to the technique are described in Sahambi *et al* (1998). Sivannarayana and Reddy (1999) have proposed the use of both launch points and wavelet extrema to obtain reliable amplitude and duration parameters from the ECG.

R wave detectors are extremely useful tools for the analysis of ECG signals. They are used both for finding the fiducial points employed in ensemble averaging analysis methods, and for computing the R–R time series from which a variety of heart rate variability (HRV) measures can be extracted (see section 3.3). Both these techniques rely on the accurate determination of the temporal location of the R wave. There are currently a number of QRS detection algorithms available which use a variety of signal analysis methods. The most common of

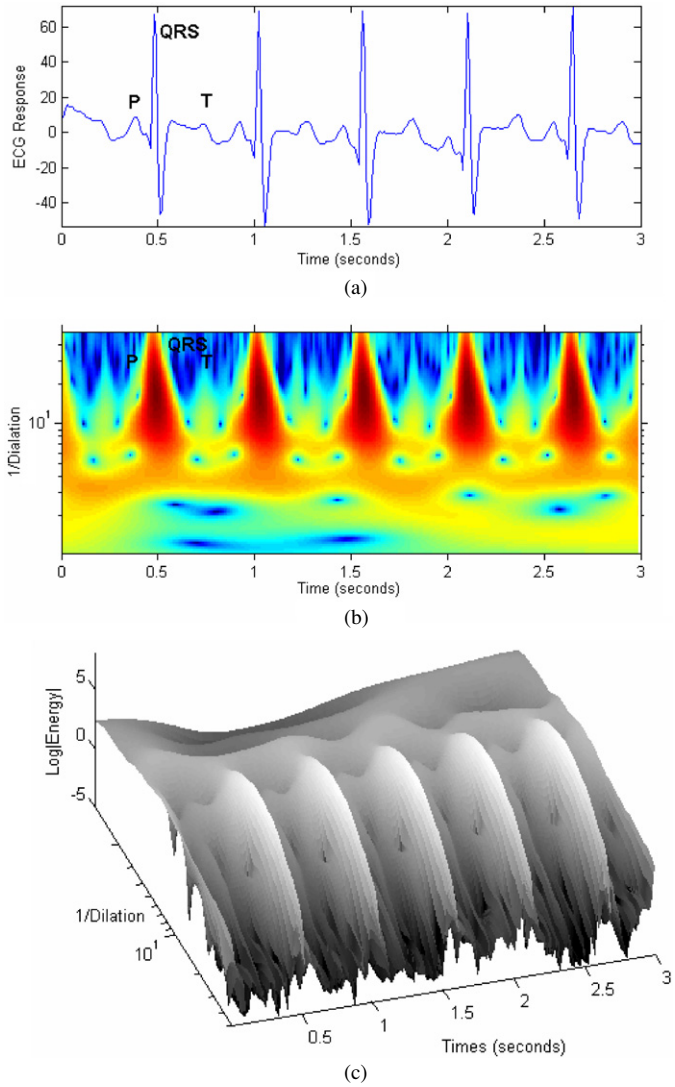

Figure 10. Wavelet transform of human sinus rhythm.

these are based on signal matched filters or time–frequency decomposition methods. Other less common methods have also been proposed including neural networks, genetic algorithms and syntactic methods (Köhler *et al* 2002). Recently, wavelet-based QRS detection methods have been suggested by a variety of groups including Li *et al* (1995) who proposed a method based on finding the modulus maxima larger than a threshold obtained from the pre-processing of preselected initial beats. In Li *et al*'s method, the threshold is updated during the analysis to obtain a better performance. This method has a post-processing phase in which redundant R waves or noise peaks are removed. The algorithm achieves a good performance with a reported sensitivity of 99.90% and positive prediction value of 99.94% when tested on the MIT/BIH database. Shyu *et al* (2004) have extended the algorithm of Li *et al* to detect ventricular premature contractions (VPCs). By incorporating a fuzzy neural network, they achieved a 99.79% accuracy for VPC classification. Martinez *et al* (2004) also utilize the algorithm of

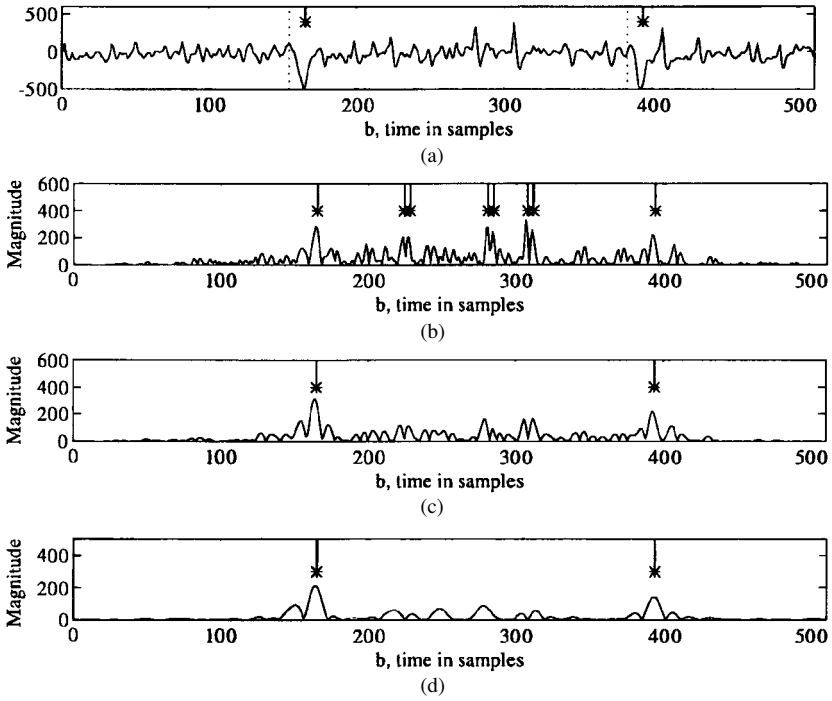

Figure 11. Tape 3203 (isolated uniform ventricular contractions (PVCs): (a) noisy portion of ECG data plotted with vertical dashed lines indicating cardiologist estimate of the QRS onset and with tick marks indicating the dyadic WT estimate of the R wave locations. (b)–(d) The dyadic WT modulus computed at scales $a = 2^1$, 2^2 and 2^3 respectively. Note the number of peaks and their locations align at scales 2^2 and 2^3. (After Kadambe *et al* 1999 *IEEE Trans. Biomed. Eng.* (© 1999 IEEE).)

Li *et al* applying a dyadic wavelet transform to a robust ECG delineation system which identifies the peaks, onsets and offsets of the QRS complexes, and P and T waves.

Kadambe *et al* (1999) have described an algorithm which finds the local maxima of two consecutive dyadic wavelet scales, and compared them in order to classify local maxima produced by R waves and by noise. Figures 11 and 12 illustrate the method which is based on the dyadic wavelet transform. Figure 11 shows a noise corrupted ECG plotted alongside a cardiologist's annotation (vertical dashed lines for the onset of the QRS). The tick marks indicate the local maxima at each scale which exceed a 60% threshold. These align themselves with the QRS peaks at scales 2 and 3. This is the basis of the Kadambe algorithm. Figure 12 shows the QRS detection for three example signals: the first including baseline wandering, the second containing a premature ventricular contraction and the third exhibiting the time varying arrhythmia known as bigeminy. Kadambe *et al* report a sensitivity of 96.84% and a positive predictive value of 95.20% when tested on a limited data set (four 30 min tapes acquired from the American Heart Association (AHA) database).

Romero Legarreta *et al* (2005) have extended the work of Li *et al* and Kadambe *et al*, utilizing the continuous wavelet transform. Their CWT-based algorithm affords high time–frequency resolution which provides a better definition of the QRS modulus maxima curves. This allows them to be followed across scales in noisy signals, and better defines the spectral region corresponding to the QRS maxima peak. Figure 13(a) shows a 5 s segment of an example ECG signal. A 3D view of the transform surface, obtained using a Mexican

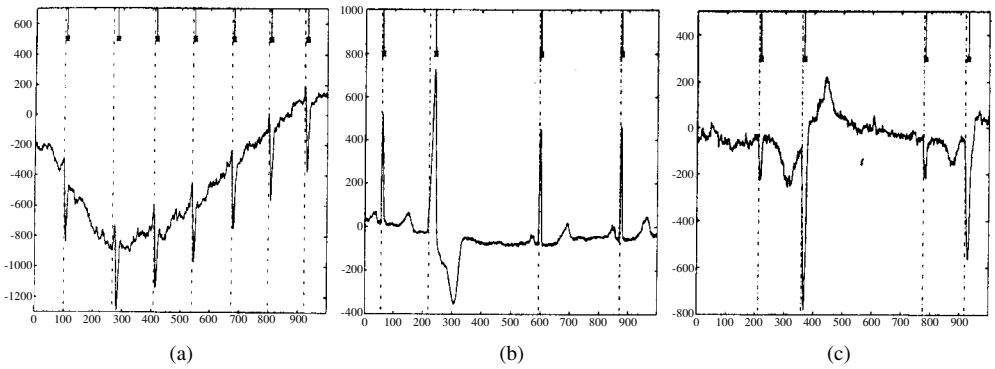

Figure 12. ECG data from AHA tapes 1209. (a) 2206, (b) 4205, (c) in (a)–(c) vertical dashed lines indicate cardiologists' estimate of the QRS onset and tic marks indicate the dyadic WT estimate of R wave locations. The horizontal axis in time in untis of samples (a) contains ECG data from tape 1209 (no PVC's) hich is corrupted by baseline wander. Tape 2206 in (b) contains portions of ECG data exhibiting an isolated uniform PVC, and (c) contains a portion of ECG data from tape 4205 exhibiting bigeminy. (After Kadambe *et al* 1999 *IEEE Trans. Biomed. Eng.* (© 1999 IEEE).)

hat wavelet, is shown below the signal. Figure 13(c) shows the modulus maxima associated with the transform surface and figure 13(d) contains a reverse view of the surface. Figure 14 shows a 3D view of the modulus maxima lines of the same signal. Each component of a single ECG complex has a different time–frequency representation that corresponds with a modulus maxima line of a specific shape. QRS complexes have more energy and higher amplitude modulus maxima lines over a longer frequency interval, whilst P and T waves have less energy and lower amplitude modulus maxima lines over a shorter frequency interval. The QRS components also have a different shape to the rest of the ECG waveform, a difference that enables simple QRS detection. Modulus maxima lines therefore act as a summary of the useful information in the CWT of the signal (Mallat 1998). Romero Legarreta *et al* used the characteristic shape of the QRS modulus maxima lines to filter out the QRS from other signal morphologies including noise and baseline wandering. Examples of their QRS detection method applied to test signals are shown in figure 15. The algorithm offers a sensitivity of 99.53% and a positive predictivity of 99.73% with signals acquired at the Coronary Care Unit at the Royal Infirmary of Edinburgh, and a sensitivity of 99.7% and a positive predictivity of 99.68% with standard signals from the MIT/BIH database.

Other work has been undertaken by Park *et al* (1998) using a wavelet adaptive filter to minimize the distortion of the ST-segment due to baseline wanderings. In a subsequent paper by Park *et al* (2001), a wavelet interpolation filter (WAF) is described for the removal of motion artefacts in the ST-segment of stress ECGs. A noise reduction method for ECG signals using the dyadic wavelet transform has been proposed by Inoue and Miyazaki (1998) and Tikkanen (1999) has evaluated the performance of different wavelet-based and wavelet packet-based thresholding methods for removing noise from the ECG. More recently, Leman and Marque (2000) have developed a wavelet packet thresholding algorithm for signal denoising algorithm, this time to remove the ECG signal from the electrohysterogram—a signal which represents uterine activity during pregnancy. Nikolaev *et al* (2001) have suppressed electromyogram (EMG) noise in the ECG using a method incorporating wavelet transform domain Wiener filtering. The method resulted in an improvement in signal-to-noise ratio of more than 10 dB. Sternickel (2002) has developed an automated P-wave detector for Holter monitors which uses multiresolution wavelet transform input to a neural network classifier.

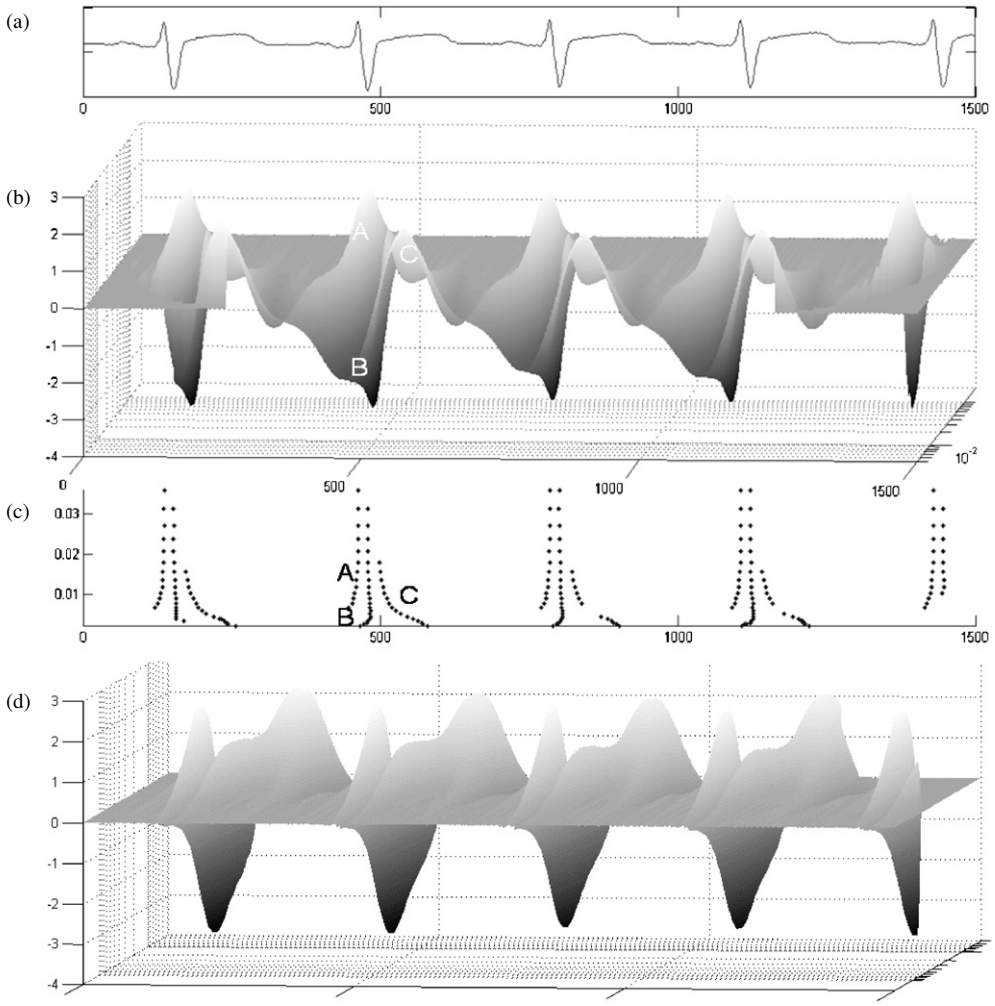

Figure 13. Continuous wavelet transform of a 3 s signal using the Mexican hat CWT. (a) Original ECG signal. (b) 3D view of the CWT. (c) Modulus maxima points above a threshold of 90% from the overall maxima. (d) Other 3D view of the CWT with the high frequencies at the front. (After Romero Legaretta *et al* 2005 *Int. J. Wavelets, Multiresolution Information Process.*).

Finally, figure 16 shows the wavelet transform scalogram plot corresponding to the ECG transition period during a pacing study (Stiles *et al* 2004). During the trial the pacemaker was set to AAI pacing mode and second degree heart block, type 1 (Wenckebach phenomenon) developed as the atrial pacing rate was increased. The ECG in the upper part of the figure initially shows a one-to-one relationship between P waves and QRS complexes, but at the half-way point it can be seen that the QRS rate abruptly slows down in an irregular fashion consistent with every third P wave not conducting through the ventricles. Although it is difficult to see the specific features in the ECG, there is a clear change in the scalogram with the onset of the heart block. The constant banding seen in the scalogram prior to the block becomes oscillatory in nature, repeating its structure synchronous with the 3:2 conduction rate. Note that the QRS features in the scalogram remain consistent across the scalogram. Figure 17, from the same study, shows a scalogram from a patient whose pacemaker was set to

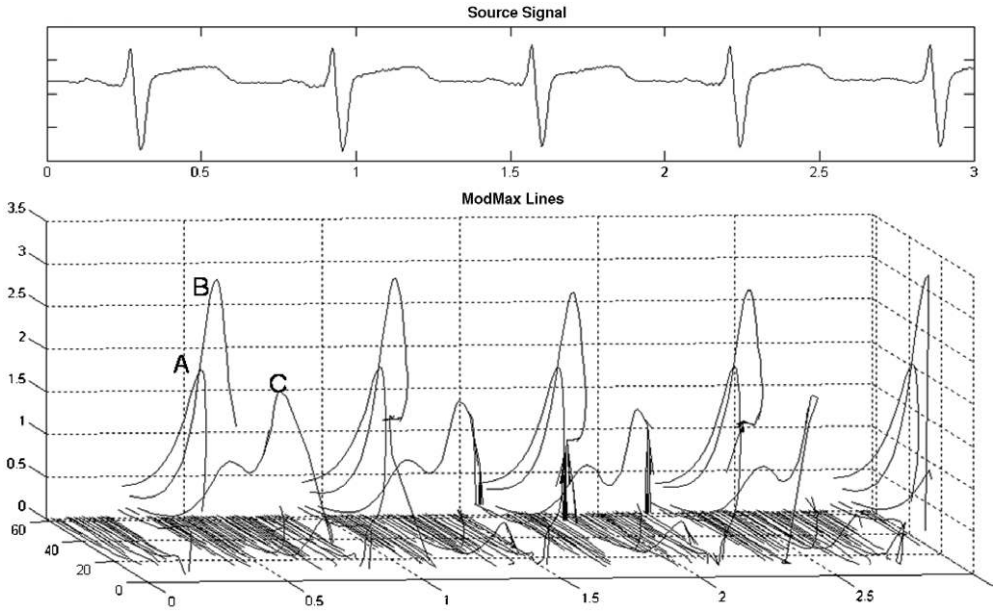

Figure 14. Modulus maxima lines of a 5 s ECG signal using the Mexican hat CWT. (After Romero Legaretta *et al* 2005 *Int. J. Wavelets, Multiresolution Information Processing*.)

DDD pacing mode and the PR interval began to exceed the programmed paced AV interval as the atrial pacing rate was increased. The ECG in the upper part of the figure shows intrinsically conducted beats, followed by 'fusion' beats where intrinsic ventricular depolarization is competing with ventricular paced beats, and finally ventricular paced beats alone without competing intrinsically conducted beats. The ridge of the wavelet band associated with the beat frequency is shown dashed on the plot. The ridge increases in frequency from $f_b = 2$ Hz to $f_m = 2.6$ Hz over the fusion region between the two arrows. This band reverts back to the pre-fusion intrinsic conduction frequency when conduction is no longer competing.

3.2. Detection of localized abnormalities

Tuteur (1989) was one of the first proponents of the wavelet transform as an analysis tool for medical signal processing, using a complex Morlet wavelet to detect abnormalities in ECG signals. In particular, Tuteur was interested in an abnormality known as a ventricular late potential (VLP). These represent low-amplitude electrical activity due to delayed electrical conduction by the ventricle muscles. VLPs occur in the ECG after the QRS complex and are often masked by noise. VLPs have been used as a marker to identify patients at risk from certain types of life threatening arrhythmias. Batista and English (1998) employed both harmonic and closely related musical wavelets in the detection of VLPs. They performed a wavelet decomposition of the ST and TP segments of the ECG and compared the relative energies contained at each level in order to detect VLPs. They reported superior results using their technique over the Simson method, widely used in clinical practice for the detection of VLPs. In addition, they found that the reduction in spectral leakage of these wavelets provides better results than using Daubechies wavelets although there is a reduction in the associated time resolution.

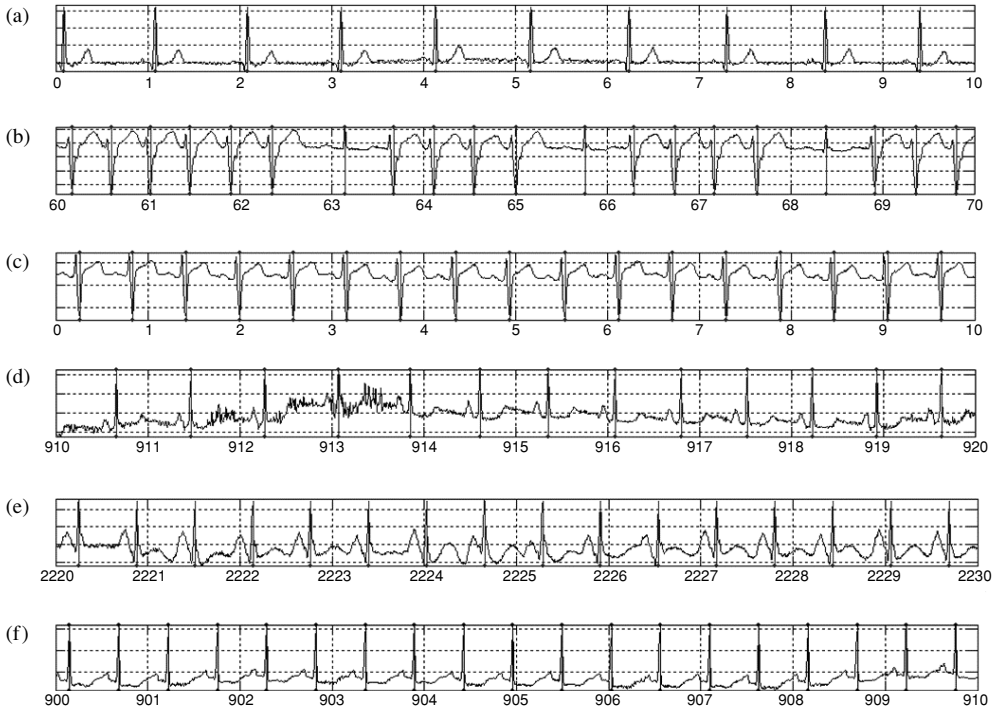

Figure 15. Examples of the wave detection algorithm. (a) ECG with very clear QRS complexes. (b) ECG with QRS complexes with very different morphologies. (c) ECG with a QRS complex with a big S wave. (d) ECG with some noise. (e) ECG with noise and high P wave. (f) ECG with clear QRS complexes and small P wave. (After Romero Legaretta *et al* 2005 *Int. J. Wavelets, Multiresolution Information Process.*)

Couderc *et al* (1996) have employed the Morlet wavelet transform to analyse high resolution ECGs in post-myocardial infarction patients both with and without documented ventricular tachycardia. A discretization of ten wavelet scales covering the relevant range of the time–frequency plane allowed them to stratify the resulting time–frequency information concerning ECG abnormalities. In the group of myocardial infarction patients with documented ventricular tachycardia they found significantly increased high-frequency components corresponding to prolonged QRS durations and late potentials in the area 80 to 150 ms after QRS onset. They also applied their method to the intra-QRS abnormalities in patients with congenital long QT syndrome. More information on their wavelet-based tools for the analysis of the ECG is given in Rubel (1996). Reinhardt *et al* (1996) have evaluated the prognostic value of their proposed wavelet correlation function of the signal-averaged ECG for arrhythmic events after myocardial infarction. The wavelet correlation function provides an autocorrelation-type measure of the wavelet transform of the signal-averaged data. By combining the wavelet correlation function with the observation of late potentials (observed in the time domain) they found an increase in the prognostic value for serious arrhythmic events after myocardial infarction (from 52% to 72% for inferior and 64% to 76% for anterior infarctions). Rakotomamonjy *et al* (1998) have detailed a method for detecting VLPs using Morlet wavelet preprocessed data as input to a feedforward neural network. They tested the technique on simulated ECGs containing VLPs and a range of additive noise and found a high degree of accuracy in classification, even for high levels of noise. Rakotomamonjy *et al* (1999)

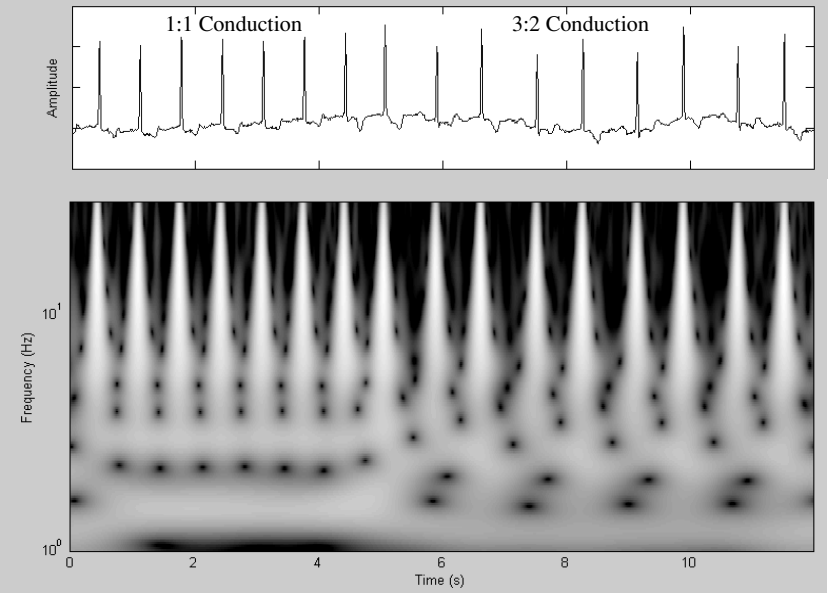

Figure 16. The Wenckebach phenomenon exhibited as the atrial pacing rate was increased. (After Stiles *et al* 2004 *Annals of Noninvasive Electrocardiology* (Blackwell Publishing).)

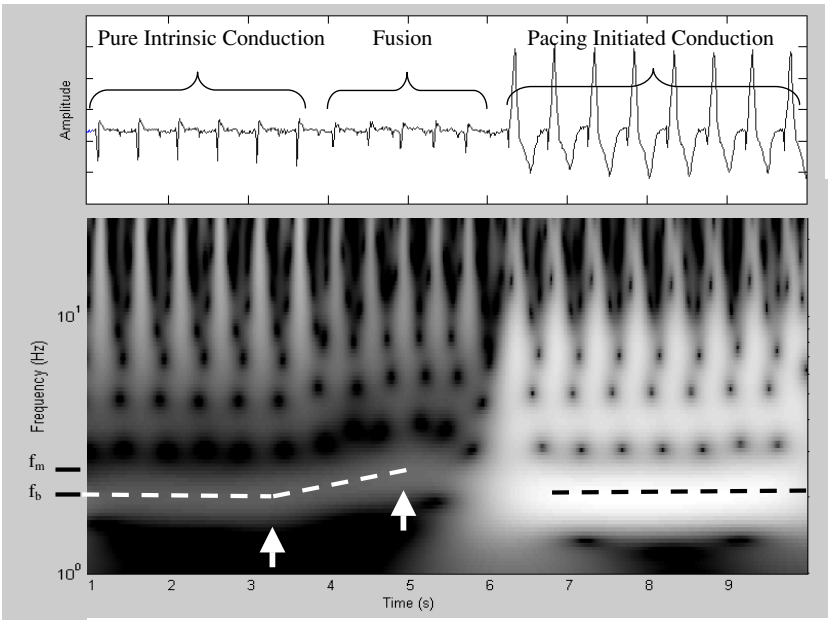

Figure 17. The onset of V pacing. (After Stiles *et al* 2004 *Annals of Noninvasive Electrocardiology* (Blackwell Publishing).)

have also described a discrete wavelet-based filtering method for signal averaged ECGs used for the detection of late potentials.

Wavelet energy scalograms were used by Meste *et al* (1994) as a method of highlighting ventricular late potentials and observing temporal and frequency variability in the ECG from

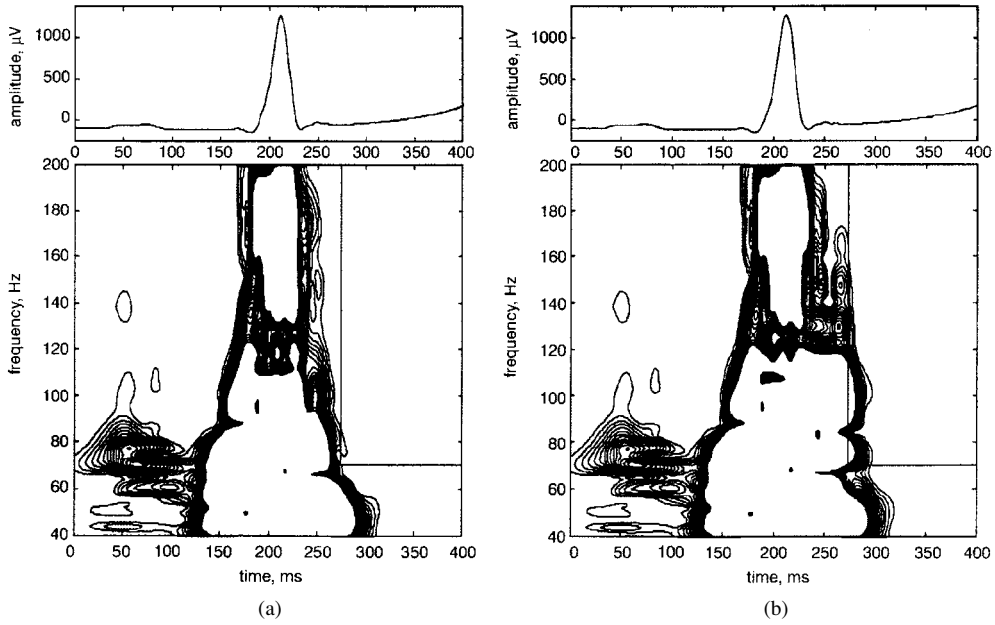

Figure 18. Averaged ECG and contour maps of wavelet transform for test signals: (a) ECG (Y-lead) of healthy subjects; (b) same signals with simulated late potentials. Time and frequency ranges for irregularity calculation are marked by straight lines. (After Lewandoswki *et al* 2000 *Med. Biol. Eng. Comput.*)

beat to beat. More recently, members of the same group have proposed a VLP detection method based on the analysis of the behaviour of the wavelet energy density surface in a selected time–frequency region occurring beyond the end of the QRS complex (Lewandowski *et al* 2000). Their method is illustrated in figure 18 where the right hand signal contains simulated late potentials. The wavelet transforms of the signals are plotted below and the region in the time–frequency plane examined for the presence of the late potentials is indicated by the box in the top right hand corner of the figure. They evaluated their method on a group of 106 post-infarction patients composed of 62 with documented monomorphic ventricular tachycardia and 44 without arrhythmia. Their results indicated that the method appears to be a useful tool for the detection of micropotentials indicating good diagnostic relevance for risk evaluation of cardiac arrhythmia. They report results of 85% sensitivity at 93% specificity for signals which were preprocessed using polynomial filtering. This result compared favourably with other methods of analysis including time domain, FFT and auto regressive methods. Wu *et al* (2001) have proposed a hybrid method which uses an artificial neural network to recognize VLPs from the (continuous) wavelet transformed signal. They report a sensitivity of 80% and specificity of 77% for the detection of beat-to-beat-based VLPs.

Popescu *et al* (1998) investigated the beat-to-beat variation of the QRS signal in post-myocardial infarction patients with sustained monomorphic ventricular tachycardia by analysing the wavelet variance distribution across the time–frequency plane. They found this measure to be a useful new estimator of ventricular tachycardia risk. In a pilot study, Gramatikov *et al* (2000) used Morlet wavelet transforms to analyse the ECG recordings from patients with left and right coronary stenosis taken before and after angioplasty. They focused on the morphology of the QRS complex in wavelet space plotting both 2D contour plots and 3D representations of the transform magnitude and demonstrated the wavelet's ability to

detect short lasting events of low amplitude superimposed on large scale deflections. The study found changes in the mid-frequency range which reflected the ECG's response to percutaneous transluminal coronary angioplasty. Link *et al* (2001) utilized both the amplitude and phase information obtained from the Morlet-based continuous wavelet transform decomposition of the ECG and MCG (magnetocardiogram) to detect the beat-to-beat variability of the QRS-complex, specifically looking for late potentials and abnormal intra-QRS potentials. They found that their technique provided a basis for distinguishing healthy patients from those prone to ventricular tachycardia of ventricular fibrillation. The detection of myocardial ischemia in pigs using a wavelet-based entropy measure is described by Lemire *et al* (2000). They considered the morphology of the combined ST segment and T wave, performing a fast wavelet transform using spline wavelets. The Shannon entropy of the coefficients at each scale was determined for the combined ST-segment–T-wave at each beat. An increase in entropy was detected at certain scales due to coronary occlusion, which led the authors to suggest a threshold entropy value as an indicator of the occlusion state. The best scale for use as a marker corresponded to an approximate frequency band of 30–60 Hz.

Chevalier *et al* (2001) used the discrete wavelet transform to identify a common electrophysiological substrate for both acquired long QT syndrome and congenital long QT syndrome. This evidence was combined with the results of imaging and genetic studies of the patients indicated a multiplicity of links between both syndromes. Olmez and Dokur (2003) employed a hybrid neural network structure in the classification of ECG signals of differing morphology, including: normal beats, left and right bundle branch block beats, premature ventricular contraction, paced beat, ventricular escape beat, fusion of ventricular and normal beats, fusion of paced and normal beats, aberrated atrial premature beat and non-conducted P waves. They reported a successful classification of 98% using discrete cosine transform preprocessing compared to 95% attained by preprocessing using a Daubechies D2 wavelet.

3.3. Heart rate variability

Rather than consider the local morphology of the whole ECG signal, many researchers have focused on the longer term temporal variability of the heartbeat, the analysis of which allows an assessment of autonomous nervous system activity (Reed *et al* 2005). The analysis of heart rate variability (HRV) requires the sequence of timing intervals between beats, taken between each R point on the QRS complex. This R–R interval can be plotted against time to give the R–R time series. In normal practice, however, ectopic beats are removed from the R–R series leaving only normal sinus beats: the N–N time series. It is this modified time series that is used in the analysis of HRV. The minute fluctuations present in the N–N intervals are used for assessing the influence of the autonomic nervous system components on the heart rate. Long range correlations and power law scaling have been found through the analysis of heartbeat dynamics. Much of the current work concerning heart rate variability focuses on its use as a marker for the prediction and diagnosis of heart disease and assessment of heart function.

The heart rate and rhythm is largely under the control of the autonomic nervous system. Traditional spectral analysis of HRV has been reported to aid the understanding of the modulatory effects of neural mechanisms on the sinus node (Malik 1996). There are three main spectral components in a traditional spectral calculation, they are generally classed as: very low frequency (VLF) ranging from 0.003 to 0.04 Hz, low frequency (LF) ranging from 0.04 to 0.15 Hz and high frequency (HF) ranging from 0.15 to 0.4 Hz components. In addition, sometimes an ultra low frequency (ULF) is defined as spectral components with frequencies less than 0.003 Hz. The relative contribution of vagal and sympathetic modulation of the heart rate is attributed to the distribution of spectral power in these bands. Over recent years,

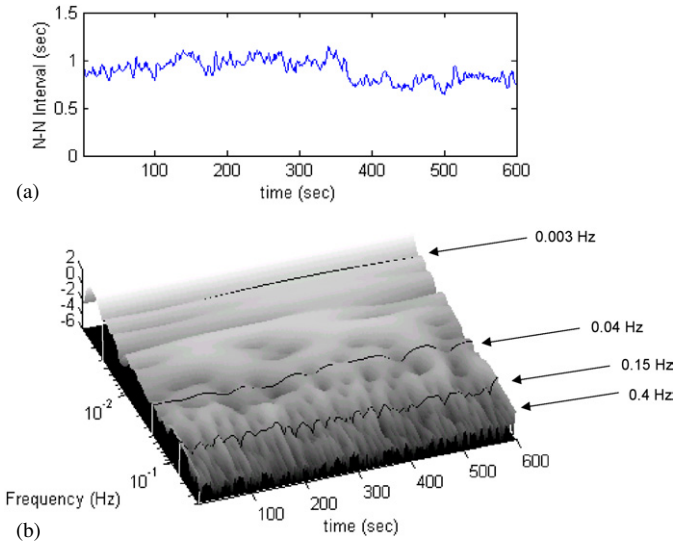

Figure 19. *N–N interval* time series from a healthy subject (top) together with its associated wavelet transform (below). The boundaries of the HF (0.4–0.15 Hz), LF (0.04–0.15 Hz) and VLF (0.003–0.04 Hz) regions are plotted across the transform surface.

a number of groups have attempted to use wavelet-based methods to gain additional insight into the mechanisms controlling heart rate variability. Figure 19 shows an example of an N–N interval time series with its associated wavelet transform surface. The N–N trace was acquired from a healthy control subject during exposure to diesel fumes as part of a study of COPD patients (Nyander *et al* 2004). The subject undertook moderate exercise half way through the 10 min trace as can be seen in the drop in N–N interval associated with the increasing heart rate. The wavelet transform surface is partitioned into the HF, LF and VLF regions whereby temporal–spectral characteristics of the surface may then be investigated.

Wiklund *et al* (1997) used adaptive wavelet transforms (wavelet packets and cosine packets) to analyse the regulation of heart rate variability (HRV) by the autonomic nervous system. Their results suggested that adapted wavelet transforms can be used to detect transient changes in the signal and characterize both tonic and reflex autonomic activity. Thurner *et al* (1998b) have employed both Daubechies D10 and Haar wavelets in the analysis of human heartbeat intervals. They found that, at distinct wavelet scales, corresponding to the interval 16–32 heartbeats, the scale-dependent standard deviations of the wavelet coefficients could differentiate between normal patients and those with heart failure. Significantly, they report 100% accuracy for a standard 27 patient data set. Further development of the technique is detailed in a subsequent paper by Thurner *et al* (1998a).

Ivanov *et al* (1996) investigated the ECG signals acquired from subjects with sleep apnoea. By sampling at an a scale equivalent to 8 heartbeats, they performed a local smoothing of the high-frequency variations in the signal in order to probe patterns of duration in the interval 30–60 s. The authors used the data to characterize the nonstationary heartbeat behaviour and elucidate phase interactions. Bates *et al* (1998) have compared two Fourier methods (the discrete Fourier transform and the nonequispaced Fourier transform) of computing the Fourier coefficients used in the discrete harmonic wavelet transform analysis of heart rate variability. The same group (Hilton *et al* 1999) have used the discrete harmonic wavelet transform as well as the discrete Fourier transform to perform spectral analysis of the HRV signals associated

with sleep apnoea/hyponeoa syndrome (SAHS). They compared their spectral analysis of the HRV signals with the current screening method of pulse oximetry. Their results indicated that spectral analysis of HRV appears to provide a better indicator of SAHS than oximetry in non-REM sleep and a comparable indicator in REM sleep. Akay and Fischer (1997) compared a wavelet-based method to others in a study to determine the fractal nature of HRV signals. Specifically, they used the method to determine the Hurst exponent of the signal. (See also Fischer and Akay (1996, 1998).) Ivanov *et al* (1999) have reported on the multifractality found in the healthy human heart rate signal using a wavelet-based analysis method. Further, they reported the loss of multifractality for a life threatening pathological condition—congestive heart failure. See also Havlin *et al* (1999) in this regard. Zhang *et al* (1997) employed techniques from nonlinear dynamics (phase space reconstruction, correlation exponent and Lyapunov exponents) to investigate heart rate variability. They applied these methods to both the R–R interval time series and to a time series of the variability of the QRS complex. Both time series were determined using the wavelet coefficients obtained from a spline wavelet decomposition of the original ECG signal. Joho *et al* (1999) analysed heart rate and left ventricular pressure variability during coronary angioplasty in humans. They presented three-dimensional, Morlet-based wavelet transform plots which showed clearly a low frequency response of both signals to coronary occlusion. They concluded that the regional myocardial ischemia elicited a profound sympathoexcitory response followed by a gradual suppression over time. This they attributed to the vagal inhibitory reflex.

Pichot *et al* (1999) used a Daubechies D4-based DWT to analyse HRV during dynamic changes in autonomous nervous system balance induced by atropine and propranolol. They favour the wavelet approach over the traditional Fourier-based approach as it 'provided novel temporally localized information'. In a later study, again using the D4 transform, Pichot *et al* (2002) analysed the nocturnal heart rate of a group of individuals subject to fatiguing exercise over a three-week period with a subsequent week of rest. They found a significant progressive decrease in the HRV indices during the three-week exercise period with a marked recovery during the rest week. In another recent study employing Daubechies D8 DWTs, Chen (2002) found that sympathovagal balance, as measured by the wavelet-based LF/HF ratio, increases prior to the onset of non-sustained ventricular tachycardia. And Gamero *et al* (2002) report on the analysis of HRV using Daubechies D12 wavelets during myocardial ischemia, their results suggesting that wavelet analysis provides useful information for the assessment of dynamic changes during this condition.

Tan *et al* (2003) have used the Morlet-based CWT in a study of the relationship between autonomic tone and spontaneous coronary spasm in patients with variant angina. They found that changes occurred in the original R–R interval time series and their wavelet-based indices before every attack indicating the imbalance in autonomic tone had occurred before ST-segment elevation.

In a recent study of early autonomic dysfunction in hypertensive offspring, Davrath *et al* (2003) report the early existence of malfunctions in both branches of autonomic control in individuals at increased risk of hypertension. They employed the continuous wavelet transform in their work and provided a real time LF and HF power and LF/HF ratio signals by integrating over the respective frequency ranges in wavelet space. Both the HR signal and blood pressure signal were used in the analysis. They showed that during periods of rest there was no difference between offspring of hypertensive parents and the control group consisting of offspring from normotensive parents. However, during the implementation of autonomic challenges which allowed abrupt transients in cardiovascular signals, subtle, yet significant, malfunctions in both branches of the autonomic nervous system were observed for the study group. In another study by the same group, again utilizing temporal LF and HF power and

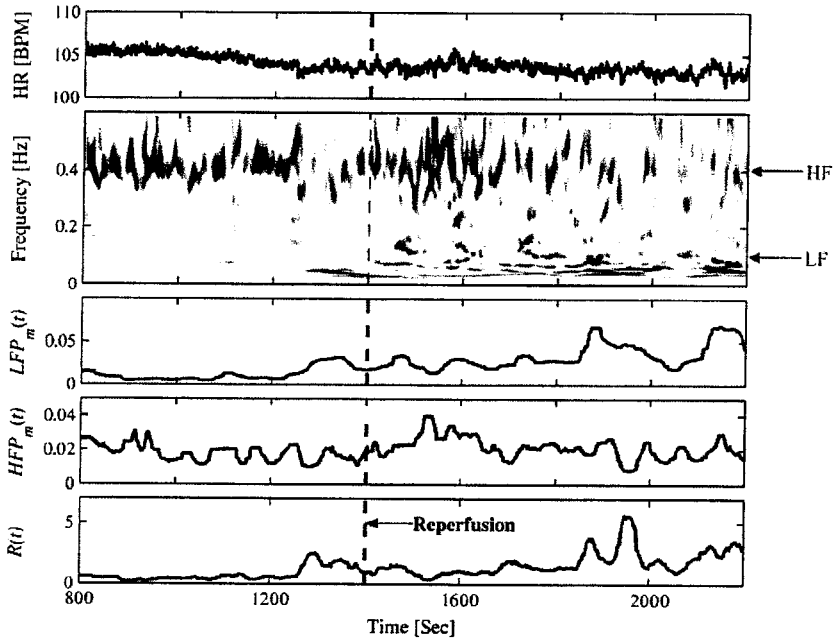

Figure 20. Wavelet analysis of patient T26 (inferoporterior wall myocardial infarction (IW-MI). Reperfusion marked by the dashed line was clinically detected at $t = 1400$ s. Note the marked increase of LFP(t) (by 380%) and $R(t)$ (by 480%) starting at $t = 1280$ s. The HFP(t) decreases slightly (7%). HR reduces by 2 beats per minute which is <2%. The increase in LFP(t) can be clearly seen in the time–frequency decomposition of the HR signal (second panel from top). The change of HRV parameters suggests a shift in cardiac autonomic activity towards sympathetic enhancement. (After Toledo *et al* 2003, used with permission.)

LF/HF ratio signals, they found that their CWT-based analysis of HRV allowed the detection of patterns directly associated with changes in myocardial perfusion (Toledo *et al* 2003). They studied the heart rate of 17 patients during thrombolysis, with reocclusion occurring in four patients. Marked alterations in their HRV parameters were found in all reperfusion and occlusion events occurring in these patients. Figure 20 illustrates their method. The figure contains the heart rate signal from a patient who suffered an inferoposterior wall myocardial infarction with its associated continuous wavelet transform plot. Below the CWT plot the low frequency power (LFP) and high frequency power (HFP) signals are plotted. These are computed by integrating over the energy density scalogram surfaces within their respective frequency ranges. The bottom signal is the ratio (R) of the LFP and HFP signals. We can see that clinical reperfusion for this patient was associated with a marked increase in both LFP and R.

Recent work by Nyander *et al* (2004) has extended the ideas of Toledo *et al* (2003) whereby individual frequency levels may be used to provide a temporal energy density signal. Further, by employing entropy measures they found that they could characterize the on/off switching of the autonomic nervous system across each frequency level. This has led them to detect a significant difference in the behaviour of COPD patients and healthy volunteers when exposed to diesel fumes during exercise. Figure 21(a) shows the rank Wilcoxon sum test for the frequency-dependent entropy marker between COPD patients during exposure to air and diesel. A significant region ($p < 0.05$) lies between 0.17 and 0.30 Hz, marked on the plot. Box plots for the entropy measure at the minimum rank Wilcoxon test value (occurring

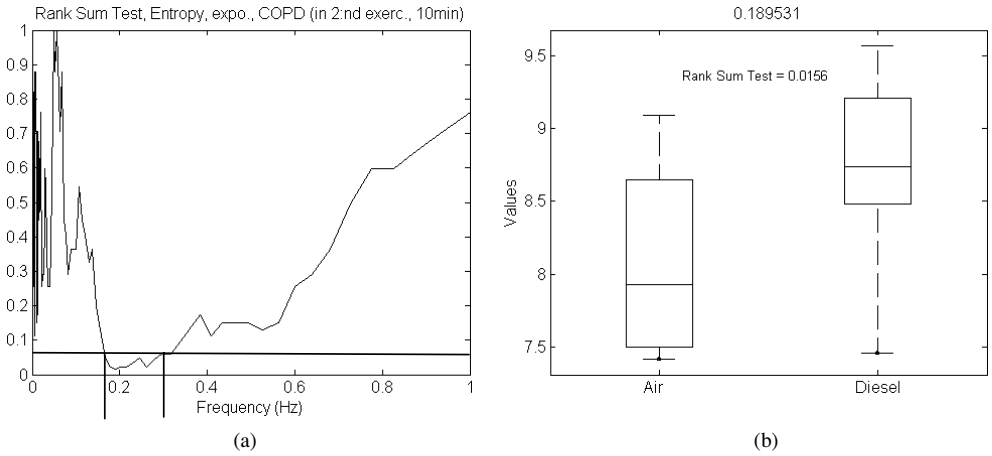

(a) (b)

Figure 21. Separation of the frequency specific entropy statistic in COPD patients during exposure to air and diesel. (a) Wilcoxon rank sum test for the entropy marker (COPD patients, signal segment B). (b) Box plots for the entropy measure at 0.190 Hz (COPD patients during exercise).

at 0.190 Hz) are presented in figure 21(b) showing the marked separation of the markers at this wavelet characteristic frequency.

3.4. Cardiac arrhythmias

A number of wavelet-based techniques have been proposed for the identification, classification and analysis of arrhythmic ECG signals. In an early paper by Govindan *et al* (1997), an algorithm is described for classifying bipolar electrograms from the right atrium of sheep into four groups—normal sinus rhythm, atrial flutter, paroxysmal atrial fibrillation (AF) and chronic AF. In their method, they use a Daubechies D6 wavelet to preprocess the ECG data prior to classification using an artificial neural network. They found paroxysmal AF the most difficult to classify with a 77% $\pm$ 9% average success rate and normal sinus rhythm the easiest, achieving 94% $\pm$ 8%. However, the study did involve small numbers in the training (10) and test (20) sets. Using a raised cosine wavelet transform, Khadra *et al* (1997) have undertaken a preliminary investigation of three arrhythmias—ventricular fibrillation (VF), ventricular tachycardia (VT) and atrial fibrillation (AF). They developed an algorithm based on the scale-dependent energy content of the wavelet decomposition to classify the arrhythmias, distinguishing them from each other and normal sinus rhythm. Again this study involved low numbers of data: 13 VF, 12 VT, 13 AF and 8 normal sinus rhythm. Zhang *et al* (1999) have proposed a novel arrhythmia detection method, based on a wavelet network, for use in implantable defibrillators. Their system, originally developed as a model to identify relationships between concurrent epicardial cell action potentials and bipolar electrogram, detects the bifurcation point in the ECG where normal sinus rhythm degenerates into a pathological arrhythmia (ventricular fibrillation). Al-Fahoum and Howitt (1999) have proposed a radial basis neural network for the automatic detection and classification of arrhythmias which employs preprocessing of the ECG using the Daubechies D4 wavelet transform. They report 97.5% correct classification of arrhythmia from a dataset of 159 arrhythmia files from three different sources, with 100% correct classification for both ventricular fibrillation and ventricular tachycardia.

Morlet *et al* (1993) presented a Morlet wavelet-based method for the discrimination of patients prone to the onset of ventricular tachycardias (VTs). They found that the detection of strings of local maxima of the wavelet transform vector at or after 98 ms after the QRS onset point was a reasonable criterion for VT risk stratification in post-infarction patients. They reported achieving 85% specificity at 90% sensitivity for their patient group. Englund *et al* (1998) studied the predictive value of wavelet decomposition of the signal-averaged ECG in identifying patients with hypertrophic cardiomyopathy at increased risk of malignant ventricular arrhythmias or sudden death. They concluded, however, that wavelet decomposition was of limited value in this type of analysis. It is interesting to note, however, that the wavelet analysis used in their study was undertaken subsequent to signal averaging of the beats. Thus intermittent local or transient aspects of the ECG can be lost to its interrogation. A later study by this group (Yi *et al* 2000) evaluated a number of wavelet decomposition parameters for their potential for risk stratification of patients with idiopathic dilated cardiomyopathy. They found that wavelet analysis was superior to time domain analysis for identifying patients at increased risk of clinical deterioration.

Atrial fibrillation (AF) is an arrhythmia associated with the asynchronous contraction of the atrial muscle fibres. It is the most prevalent cardiac arrhythmia in the western world, and is associated with significant morbidity. Duverney *et al* (2002) have developed a combined wavelet transform–fractal analysis method for the automatic detection of atrial fibrillation from heart rate intervals. After training their method on healthy sinus rhythm and chronic AF ECGs, they achieved 96.1% sensitivity at 92.6% specificity for discriminating AF episodes in paroxysmal AF. Figures 22 and 23 illustrate a technique for the elucidation of AF from within an ECG signal using a modulus maxima denoising technique (Watson *et al* 2001). Figure 22 shows the wavelet transform decomposition of a 2 s segment of ECG from a patient with atrial fibrillation. Below the trace is a scalogram plot, obtained using a Mexican hat-based wavelet transform. This yields high temporal resolution in the wavelet domain, but generates a very large data set. The corresponding modulus maxima are plotted below the scalogram. As can be seen from the figure, dominant modulus maxima lines at the scale of 10 Hz and below are almost solely associated with the coherent QRS and T structures. Therefore, the modulus maxima lines at this scale with a high proportion of the total energy within this scale are selected. The selected modulus maxima lines are then followed across scales and subtracted to leave a residual signal associated with both system noise and, more importantly, atrial activity. An inverse transform, performed separately on both sets of retained maxima lines, recovers the partitioned signals. This time–frequency partitioning of the signal results in two components: one (1) containing combined low and high frequency components that correspond to large scale features in the signal, and a second (2) containing the remaining high frequency components that correspond to small scale AF features and noise. In practice, most applications are concerned with signal denoising and hence the retention of component (1). This application, however, is concerned with the removal of large amplitude features to allow examination of the lower amplitude AF components of the signal, and hence component (2) is retained for analysis. Figure 23 contains a 7 s segment of ECG taken during a pilot study of patients with AF. The signal has been partitioned using the modulus maxima technique described above where the modulus maxima have been separated into large and small scale features. An enlarged part of the signal is given in the lower three plots in the figure. The middle plot contains the partitioned signal with the QRS complex and T wave filtered out, revealing regular, coherent features that appear at a frequency of approximately 400 beats per minute, often seen during invasive studies of atrial activity in patients with AF. The lower plot contains the partition with the filtered out QRS and T waves. Although a relatively simple modulus maxima technique was used, whereby the modulus maxima lines were simply

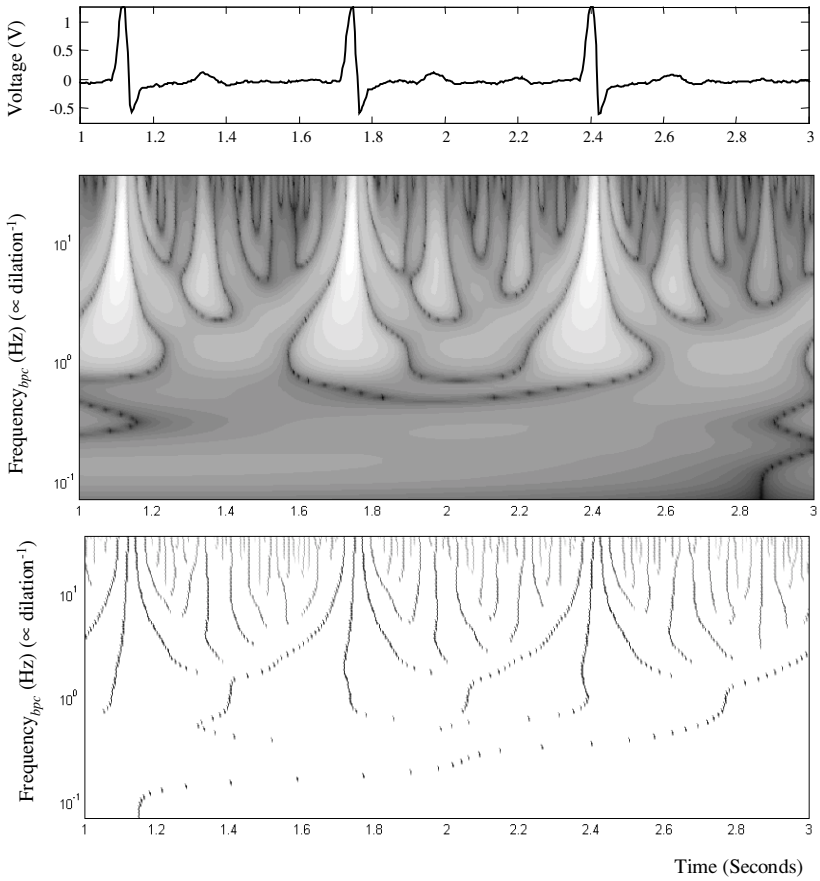

Figure 22. ECG trace exhibiting AF (top) together with its associated scalogram (middle) and modulus maxima plot (bottom). (After Watson *et al* 2001 (© 2001 IEEE).)

partitioned into two subsets, the ability of the technique to separate the signal into QRS and T waves and underlying AF is evident from the preliminary results.

Ventricular tachyarrhythmias, and in particular ventricular fibrillation (VF), are the primary arrhythmic events in the majority of patients who present with sudden cardiac death. During ventricular fibrillation the lower chambers of the heart beat in an irregular fashion. Much work has been conducted over recent years into VF centred on attempts to understand the pathophysiological processes occurring in sudden cardiac death, predicting the efficacy of therapy, and guiding the use of alternative or adjunct therapies to improve resuscitation outcomes (Reed *et al* 2003). A global view of a long term VF signal in wavelet space is given in figure 24 which contains an energy scalogram for a 5 min period of pig VF followed by a 2.5 min period of cardiopulmonary resuscitation (CPR). The onset of CPR is distinguished by the large amplitude horizontal band appearing at low frequency at 5 min. Distinct banding can be seen in the scalogram over the first 5 min: a high frequency band at around 10 Hz and two lower energy bands at lesser frequencies labelled A, B and C. After the onset of CPR, a gradual increase in the frequency of all three bands over about a minute can be observed in the scalogram. Note that these increasing bands (varying in frequency over time) are obviously decoupled from the constant-frequency CPR band, and are not therefore an artefact of the signal processing. These bands indicate a gradual increase in the underlying frequency of

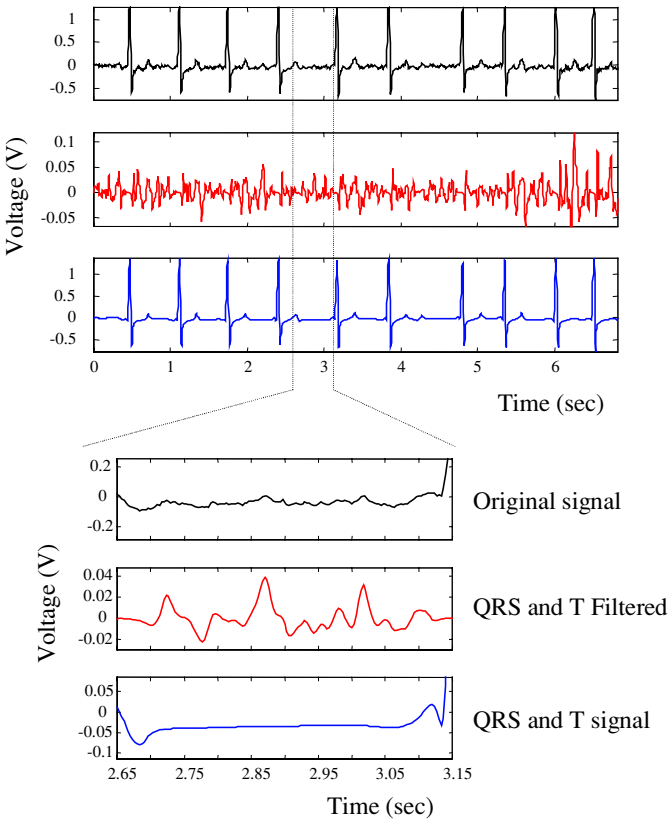

Figure 23. Wavelet filtering of the ECG exhibiting AF. (After Watson *et al* 2001 (© 2001 IEEE).)

fibrillation over a period of about 1 min caused by the administration of CPR (Addison *et al* 2000).

Figure 25 shows the pressure in the aorta and ECG corresponding to an episode of ventricular fibrillation in another porcine model. The ECG signal has a typical random or unstructured appearance. The aorta pressure trace, however, reveals regular low amplitude spikes. On opening the chest of this animal and observing the heart directly, it became apparent that the ventricles were fibrillating, but the atria were contracting independently in a co-ordinated manner (Addison *et al* 2002a). The irregular activity of the much larger ventricular muscle mass completely obscured this atrial activity in the standard ECG recording shown in the second top plot of figure 25. The wavelet energy scalogram for this signal is plotted below the ECG signal. (A Morlet wavelet was used in the study.) The high amplitude band at around 8–10 Hz is much more compact in extent in frequency than that found for other traces where no atrial pulsing was apparent. Furthermore, there is some evidence of 'pulsing' in this band between 1 and 2 Hz in the scalogram. This is confirmed in the bottom plot of figure 25 where the location of zero wavelet phase is plotted over a short range of the bandpass frequencies, between 1.1 and 1.5 Hz. Below this zero phase plot is the pressure tracing. The phase plot exhibits a strikingly regular pattern with the zero phase lines aligning themselves remarkably well with the atrial pulsing of the pressure trace. This result suggests that (wavelet) phase information, obscure to traditional methods, may be used to interrogate the ECG for underlying low-level mechanical activity in the atria.

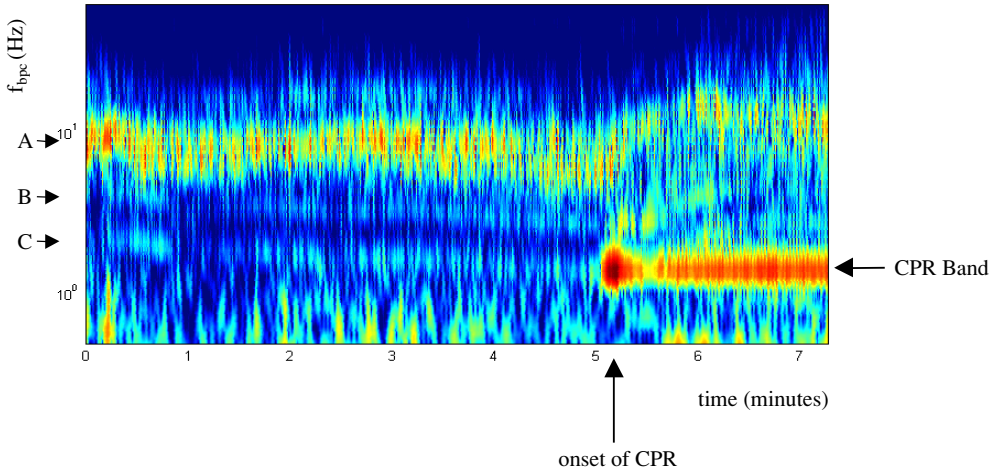

Figure 24. The energy scalogram for the first 7 min of porcine ventricular fibrillation. CPR is initiated at 5 min as indicated. (After Addison *et al* 2000 (© 2000 IEEE).)

Many researchers have used animal models in the study of VF. This allows laboratory study of this fatal arrhythmia, in particular the acquisition of long term VF data sets. The validity of this approach is questionable, both in terms of the underlying pathophysiology, and because significant interspecies differences in parameters such as median fibrillation frequency invalidate direct extrapolation to the human situation. Although these models still provide important information on the long term aspects of VF, much work has focused on the analysis of short term traces of pre-shock human VF obtained from out of hospital cardiac arrests acquired through modified defibrillator devices. Coherent spiking structure has also been observed in these segments of human VF. An example of this is shown in figure 26 where the ECG signal in the vicinity of a shock is plotted. The preshock VF exhibits distinct high-frequency spiking activity in wavelet space (indicated by the arrows in the plot). The observation reveals that human VF, previously thought to represent disorganized and unstructured electrical activity of the heart, does in fact contain a rich underlying structure hidden to traditional Fourier techniques (Addison *et al* 2000, Watson *et al* 2000). Building upon these results, a wavelet-based method for the prediction of the outcome from defibrillation shock in human VF has recently been proposed by Watson *et al* (2004). An enhanced version of this method (Watson *et al* 2005) employing entropy measures of selected modulus maxima achieves well over 60% specificity at 95% sensitivity for predicting a return of spontaneous circulation (ROSC). This is significantly better than current alternative techniques based on a variety of measures including Fourier, fractal, angular velocity, etc. The best of these typically achieves 50% specificity at 95% sensitivity. This enhancement is due to the ability of the wavelet transform to isolate and extract specific spectral–temporal features for use in the analysis. Thus, whereas the proposed alternative methods all characterize behaviour over time (even although for short periods) the wavelet transform can selectively pull pertinent information out in time. This is done through a novel entropy-based measure applied to pre-filtered modulus maxima lines. The incorporation of such outcome prediction technologies within defibrillation devices will significantly alter their function as current standard protocols, involving sequences of shocks and CPR, can be altered depending on the likelihood of success of a shock. If there is a high probability of success a shock-first approach will be adopted, whereas if there is a substantially low likelihood of success, then an alternative therapy prior

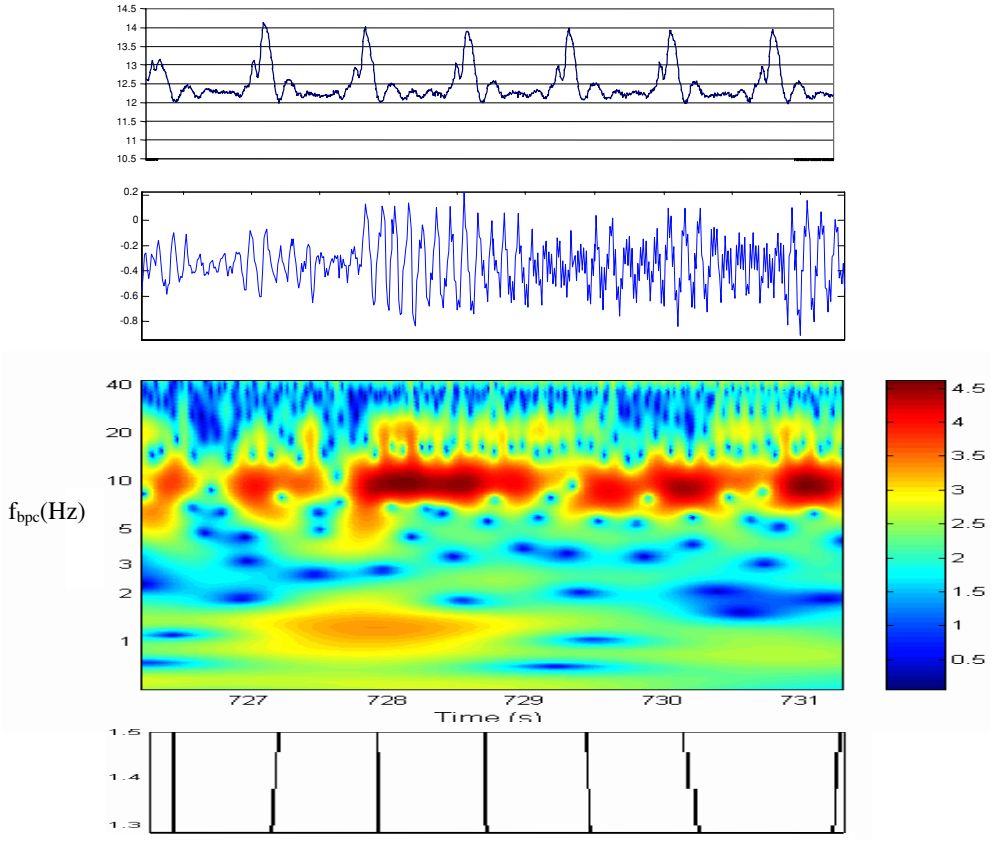

Figure 25. Simultaneous ECG and pressure recordings. The aorta pressure trace (top), with ECG (second top), corresponding wavelet energy plot (second bottom) obtained using the Morlet wavelet. The zero phase lines of the Morlet wavelet transform (bottom). The plots correspond to the time period 726.23–731.31 s after the initiation of VF. (After Addison *et al* 2002 *IEEE Eng. Med. Biol.* (© IEEE 2002).)

to shock will be used (e.g. CPR and/or a drug) to stimulate the heart and enhance its condition prior to shocking.

3.5. ECG data compression

ECG signals are collected both over long periods of time and at high resolution. This creates substantial volumes of data for storage and transmission. Data compression seeks to reduce the number of bits of information required to store or transmit digitized ECG signals without significant loss of signal quality. Many schemes have been proposed for this task. These can be categorized as either direct methods or transform methods. Direct methods involve the compression performed directly on the ECG signal. Transform methods, as their name implies, operate by first transforming the ECG signal into another domain including Fourier, Walsh, Kahunen Loeve, discrete cosine transforms and more recently the wavelet transform (Jalaleddine *et al* 1990). An early paper by Crowe *et al* (1992) suggested the wavelet transform as a method for compressing both ECG and heart rate variability data sets. Thakor *et al* (1993a) compared two methods of data reduction on a dyadic scale for normal and abnormal cardiac rhythms, detailing the errors associated with increasing data reduction ratios. Using discrete

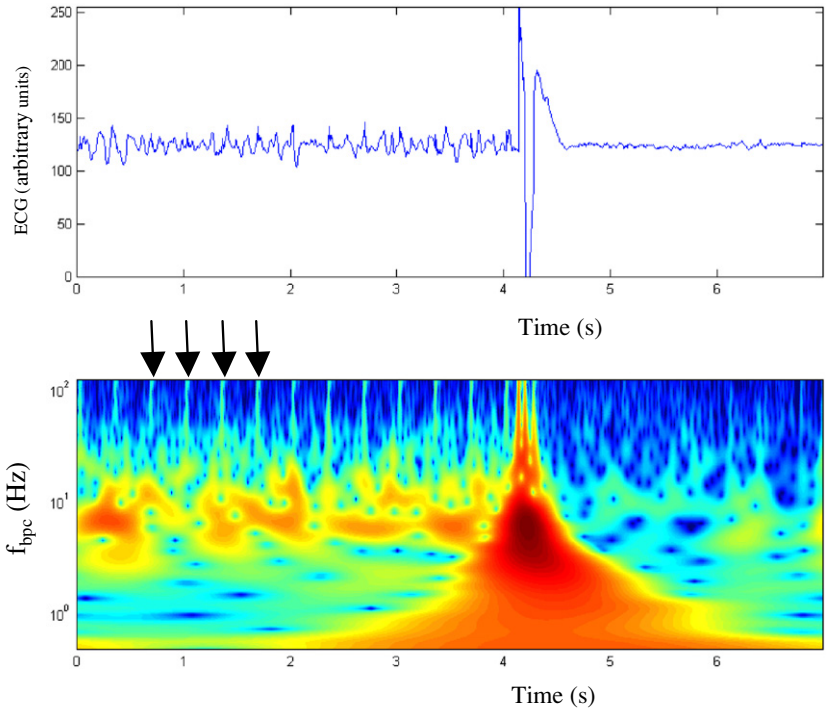

Figure 26. Attempted defibrillation of human ventricular fibrillation. Top: 7 s of human ECG exhibiting VF containing a defibrillation shock event. Bottom: scalogram corresponding to the ECG signal. Note the high frequency spiking prior to the shock evident in the scalogram—indicated by arrows. (After Addison *et al* 2002 *IEEE Eng. Med. Biol.* © IEEE 2002.)

orthonormal wavelet transforms and Daubechies D10 wavelets, Chen *et al* (1993) compressed ECG data sets resulting in compression ratios up to 22.9:1 while retaining clinically acceptable signal quality. In a later paper (Chen and Itoh 1998), again using D10 wavelets, they incorporate an adaptive quantization strategy which allows a predetermined desired signal quality to be achieved. Miaou and Lin (2000) also propose a quality driven compression methodology based on Daubechies wavelets and later (Miaou and Lin 2002) on biorthogonal wavelets. The latter algorithm adopts the set partitioning of hierarchical tree (SPIHT) coding strategy. Miaou *et al* (2002) have also proposed a dynamic vector quantization method employing tree codevectors in a single codebook. Some examples of original and compressed signals from this work are shown in figure 27.

Bradie (1996) suggested the use of a wavelet-packet-based algorithm for compression of the ECG. When compared to the Karhunen–Loeve transform (KLT) applied to the same data the WP method generated significantly lower data rates at less than one-third the computational effort with generally excellent reconstructed signal quality. However, Blanchett *et al* (1998) report at least as good compression results for a KLT-based method. By first normalizing beat periods using multirate processing and normalizing beat amplitudes Ramakrishnan and Saha (1997) converted the ECG into a near cyclostationary sequence. They then employed a uniform choice of significant Daubechies D4 wavelet transform coefficients within each beat thus reducing the data storage required. Their method encodes the QRS complexes with an error equal to that obtained in the other regions of the cardiac cycle.

Popescu *et al* (1999) have developed a multiresolution distributed filtering data reduction method for high resolution ECG signals (HRECGs) used in the assessment of ventricular

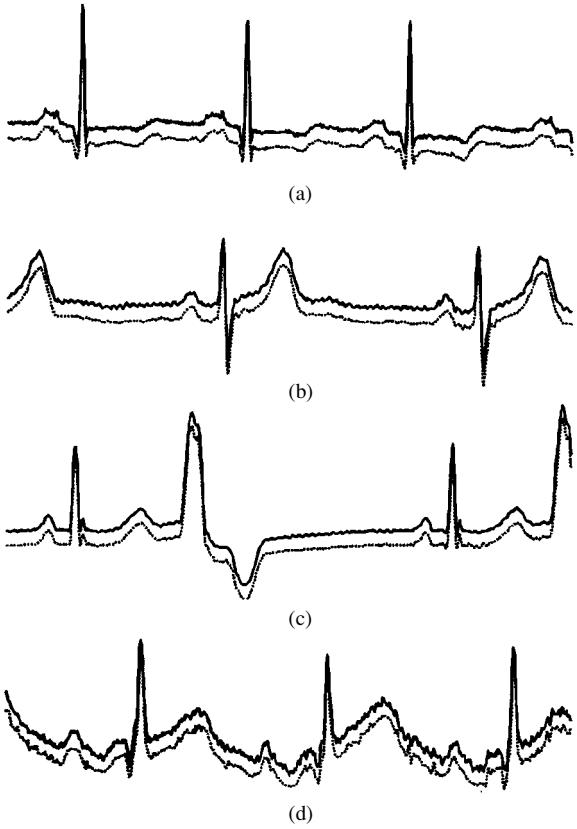

Figure 27. Typical waveform segments of original (solid line) and reconstructed (dashed line) signals. (After Miaou *et al* 2002 (© 2002 IEEE).)

tachycardia risk in post-myocardial infarction patients. The method employs adaptive Bayesian shrinkage of the wavelet coefficients prior to reconstruction which allows a significant reduction in data required to represent the signals. The method is particularly suited to HRECGs which are often used to detect small-amplitude late potentials, which are established arrhythmogenic markers in this group of patients. The authors found the Bayesian method superior to hard and soft wavelet thresholding techniques as well as other established non-wavelet methods.

A comparison of the performance of the many ECG compression methods—wavelets and other—can be found in the paper by Cárdenas-Barrera and Lorenzo-Ginori (1999). More recent data compression schemes for the ECG include the method using non-orthogonal wavelet transforms by Ahmed *et al* (2000) and the set partitioning in hierarchical trees (SPIHT) algorithm employed by Lu *et al* (2000).

Istepanian and Petrosian (2000) describe the implementation of a mobile telecardiology system based on their optimal zonal wavelet coding (OZWC) wavelet transform compression technique. They found that compression ratios of up to 18:1 could be achieved without reducing the clinical quality of the transmitted ECG whilst retaining the necessary features for clinical diagnosis at the receiver end. A more recent paper by Istepanian *et al* (2001) compares the OZWC method with their wavelet transform higher order statistics-based coding (WHOSC) scheme. They found that although the WHOSC scheme produced higher compression ratios

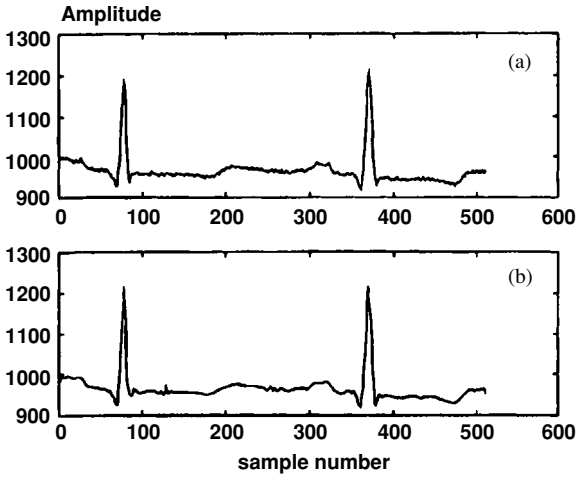

Figure 28. Reconstruction results of the OZWC algorithm on a section from the MIT100 record. (a) Original ECG, (b) reconstructed ECG. (After Istepanian *et al* 2001 (© 2001 IEEE).)

it had poorer normalized rms error when compared with the OZWC method. Both methods can be used for mobile telemedical applications. Figure 28 shows an original segment of ECG together with an ECG reconstructed using the OZWC algorithm.

4. Discussion and concluding remarks

The wavelet transform has emerged over recent years as a key time–frequency analysis and coding tool for the ECG. As we have seen in this review, its ability to separate out pertinent signal components has led to a number of wavelet-based techniques which supersede those based on traditional Fourier methods. In its continuous form, the CWT allows a powerful analysis of non-stationary signals, making it ideally suited for the high-resolution interrogation of the ECG over a wide range of applications. In its discrete form, the DWT and its offshoots, the SWT and WPT, provide the basis of powerful methodologies for partitioning pertinent signal components which serve as a basis for potent compression strategies.

It is interesting to note that researchers coming to the wavelet transform tend to take an either/or approach to their study: either concentrating on the DWT or the CWT. Relatively few explore both in depth. The DWT has interesting mathematics and fits in with standard signal filtering and encoding methodologies. It produces few coefficients, its practical application is simple with many off-the-shelf software toolboxes available (e.g. Matlab Wavelet Toolbox®), and the user does not have to worry about losing energy during the transform process or its inverse. However, it exhibits non-stationarity and coarse time–frequency resolution. The CWT, on the other hand, allows arbitrarily high resolution of the signal in the time–frequency plane, which is a necessity for the accurate identification and partitioning of pertinent components. However, the discretization of the continuous wavelet transform, required for its practical implementation with discrete signals, involves a discrete approximation of the transform integral (i.e. a summation) computed on a discrete (but not dyadic) grid of a scales and b locations. The inverse continuous wavelet transform is also computed as a discrete approximation. How close an approximation to the original signal is recovered depends mainly on the resolution of the discretization used and, with care, usually a very good approximation can be recovered. CWT algorithms are widely available, however, the inverse CWT algorithm is not available in standard software toolboxes: you have to write your own!

This either/or approach, evident in the literature, has led to a number of papers appearing where the discrete transform has been used in the analysis of the signal, whereby the coarseness of the resulting decomposition makes identification of pertinent features within the transform difficult, if not practically impossible. The non-stationarity of the DWT can also cause problems in terms of repeatability and robustness of the analysis, unless it particularly lends itself to an ensemble averaged method. Although the stationary wavelet transform can overcome this, it is still limited to dyadic frequency scales and involves significantly more coefficients than the DWT.

The author expects that the future will see the application of the CWT to many of the problems that the DWT (or SWT) has previously been applied to. The often cited argument for using the DWT in an analysis role, because the CWT is significantly more expensive computationally, is most often a spurious one: especially true given the computing power now generally available—even in fairly basic medical devices. It is also envisaged that further study of techniques for compacting the information contained in the CWT into a tiny subset of coefficients, such as modulus maxima, ridge following and perhaps even reassignment methods (Clifton *et al* 2003), will lead to further novel CWT-based analysis and compression techniques in the future.

In conclusion, it has been shown that the wavelet transform is a flexible time–frequency decomposition tool which can form the basis of useful signal analysis and coding strategies. It is envisaged that the future will see further application of the wavelet transform to the ECG as the emerging technologies based on them are honed for practical purpose.

Additional information

The wavelet newsgroup, *Wavelet Digest*, is an e-mail periodical and associate website (www.wavelet.org) which contains news and views from the wavelet community including details of new books, conferences, papers, recent theses, software, courses and so on. The Wavelet Digest contains much useful information for novice and expert alike.

References

Abramovich F, Bailey T C and Sapatinas T 2000 Wavelet analysis and its statistical implications *Statistician* **49** 1–29

Addison P S 1999 Wavelet analysis of the breakdown of a pulsed vortex flow *Proc. Inst. Mech. Eng.* C **213** 217–29

Addison P S 2002 *The Illustrated Wavelet Transform Handbook: Introductory Theory and Applications in Science Engineering, Medicine and Finance* (Bristol: Institute of Physics Publishing)

Addison P S and Watson J N 2004 Secondary transform decoupling of shifted nonstationary signal modulation components *Int. J. Wavelets, Multiresolution Inf. Process.* **2** 43–57

Addison P S, Watson J N, Clegg G R, Holzer M, Sterz F and Robertson C E 2000 Evaluating arrhythmias in ECG signals using wavelet transforms *IEEE Eng. Med. Biol.* **19** 104–9

Addison P S, Watson J N, Clegg G R, Steen P A and Robertson C E 2002a Finding coordinated atrial activity during ventricular fibrillation using wavelet decomposition *IEEE Eng. Med. Biol.* **21** 58–65

Addison P S, Watson J N and Feng T 2002b Low-oscillation complex wavelets *J. Sound Vib.* **254** 733–62

Ahmed S M, Al-Shrouf A and Abo-Zahhad M 2000 ECG data compression using optimal non-orthogonal wavelet transform *Med. Eng. Phys.* **22** 39–46

Akay M and Fischer R 1997 Fractal analyses of HRV signals: a comparative study *Methods Inf. Med.* **36** 271–3

Al-Fahoum A S and Howitt I 1999 Combined wavelet transformation and radial basis neural networks for classifying life-threatening cardiac arrhythmias *Med. Biol. Eng. Comput.* **37** 566–73

Arneodo A, d'Auberton-Carafa Y, Audit B, Bacry E, Muzy J F and Thermes C 1998 Nucleotide composition effects on the long-range correlations in human genes *Eur. Phys. J.* B **1** 259–63

Bates R A, Hilton M F, Godfrey K R and Chappell M J 1998 Comparison of methods for harmonic wavelet analysis of heart rate variability *IEE Proc. Sci. Meas. Technol.* **145** 291–300

Batista A and English M 1998 Ventricular late potential analysis with musical and harmonic wavelets *Med. Eng. Phys.* **20** 773–9

Blanchett T, Kember G C and Fenton G A 1998 KLT-based quality controlled compression of single-lead ECG *IEEE Trans. Biomed. Eng.* **45** 942–5

Blatter C 1998 *Wavelets: A Primer* (Natick, MA: AK Peters)

Bradie B 1996 Wavelet packet-based compression of single lead ECG *IEEE Trans. Biomed. Eng.* **43** 493–501

Bruce L M and Adhami R R 1999 Classifying mammographic mass shapes using the wavelet transform modulus-maxima method *IEEE Trans. Med. Imaging* **18** 1170–7

Cárdenas-Barrera J L and Lorenzo-Ginori J 1999 Mean-shape vector quantizer for ECG signal compression *IEEE Trans. Biomed. Eng.* **46** 62–70

Carmona R A, Hwang W L and Torresani B 1997 Characterization of signals by the ridges of their wavelet transform *IEEE Trans. Signal Process.* **45** 2586–90

Chen J and Itoh S 1998 A wavelet transform-base ECG compression method guaranteeing desired signal quality *IEEE Trans. Biomed. Eng.* **45** 1414–9

Chen J, Itoh S and Hashimoto T 1993 ECG data compression by using wavelet transform *IEICE Trans. Inf. Syst.* **E76D** 1454–61

Chen S-W 2002 A wavelet-based heart-rate variability analysis for the study of nonsustained ventricular tachycardia *IEEE Trans. Biomed. Eng.* **49** 736–42

Chevalier P, Rodriguez C, Bontemps L, Miquel M, Kirkorian G, Rousson R, Potet F, Schott J-J, Baro I and Touboul P 2001 Non-invasive testing of acquired long QT syndrome: evidence for multiple arrhythmogenic substrates *Cardiovasc. Res.* **50** 386–98

Clifton D, Addison P S, Styles M, Romero Legaretta I, Grubb N R, Watson J N, Clegg G R and Robertson C E 2003 Using wavelet transform reassignment techniques for ECG characterisation *Computers in Cardiology (Thessaloniki, Greece, 21–24 Sept. 2003)*

Coifman R R and Donoho D L 1995 Translation invariant de-noising *Lect. Notes Statist.* **103** 125–50

Collineau S and Brunet Y 1993 Detection of turbulent coherent motions in a forest canopy: part 1. Wavelet analysis *Bound.-Layer Meteorol.* **65** 357–79

Couderc J P, Fareh S, Chevalier P, Fayn J, Kirkorian G, Ruberl P and Touboul P 1996 Stratification of time–frequency abnormalities in the signal averaged high-resolution ECG in postinfarction patients with and without ventricular tachycardia and congenital long QT syndrome *J. Electrocardiol.* **29** (Suppl.) S180–8

Crowe J A, Gibson N M, Woolfson M S and Somekh M G 1992 Wavelet transform as a potential tool for ECG analysis and compression *J. Biomed. Eng.* **14** 268–72

Daubechies I 1992 *Ten Lectures on Wavelets (CBMS-NSF Regional Conf. Ser. in Applied Mathematics)* (Philadelphia, PA: SIAM)

Davrath L R, Goren Y, Pinhas I, Toledo E and Akselrod S 2003 Early autonomic malfunction in normotensive individuals with a genetic predispositiojn to essential hypertension *Am. J. Physiopl. Heart Circ. Physiol.* **285** H1697–704

Delprat N, Escudie B, Guillemain P, Kronland-Martinet R, Tchamitchain P and Torresani B 1992 Asymptotic wavelet and Gabor analysis: extraction of instantaneous frequencies *IEEE Trans. Inf. Theory* **38** 644–64

Dupuis P and Eugene C 2000 Combined detection of respiratory and cardiac rhythm disorders by high-resolution differential cuff pressure measurement *IEEE Trans. Instrum. Meas.* **49** 498–502

Duverney D, Gaspoz J-M, Pichot V, Roche F, Brion R, Antoniadis A and Barthelemy J-C 2002 High accuracy of automatic detection of atrial fibrillation using wavelet transform of heart rate intervals *PACE* **25** 457–62

Englund A, Hnatkova K, Kulakowski P, Elliot P M, McKenna W J and Malik M 1998 Wavelet decomposition analysis of the signal averaged electrocardiogram used for risk stratification of patients with hypertrophic cardiomyopathy *Eur. Heart J.* **19** 1383–90

Fischer R and Akay M 1996 A comparison of analytical methods for the study of fractional Brownian motion *Ann. Biomed. Eng.* **24** 537–43 chapter 6/chapter 7

Fischer R and Akay M 1998 Fractal analysis of heart rate variability *Time Frequency and Wavelets in Biomedical Signal Processing* ed M Akay (New York: IEEE) chapter 6/chapter 7 pp 719–28

Gamero L G, Vila J and Palacios F 2002 Wavlet transform analysis of heart rate variability during myocardial ischemia *Med. Biol. Eng. Comput.* **40** 72–8

Goupillaud P, Grossmann A and Morlet J 1984 Cycle-octave and related transforms in seismic signal analysis *Geoexploration* **23** 85–102

Govindan A, Deng G and Power J 1997 Electrogram analysis during atrial fibrillation using wavelet and neural network techniques *Proc. SPIE* **3169** 557–62

Gramatikov B, Brinker J, Yi-chun S and Thakor N V 2000 Wavelet analysis and time-frequency distributions of the body surface ECG before and after angioplasty *Comput. Methods Prog. Biomed.* **62** 87–98

Guilbaud S and Audoin B 1999 Measurement of the stiffness coefficients of a viscoelastic composite material with laser generated and detected ultrasound *J. Acoust. Soc. Am.* **105** 2226–35

Hadjileontiadis L J and Panas S M 1997 Separation of discontinuous adventitious sounds from vesicular sounds using a wavelet-based filter *IEEE Trans. Biomed. Eng.* **44** 1269–81

Havlin S, Amaral L A N, Ashkenazy Y, Goldberger A L, Ivanov P C, Peng C-K and Stanley H E 1999 Application of statistical physics to heartbeat diagnosis *Physica* A **274** 99–110

Higuchi H, Lewalle J and Crane P 1994 On the structure of a two-dimensional wake behind a pair of flat plates *Phys. Fluids* **6** 297–305

Hilton M F, Bates R A, Godfrey K R, Chappell M J and Cayton R M 1999 Evaluation of frequency and time–frequency spectral analysis of heart variability as a diagnostic marker of sleep apnoea syndrome *Med. Biol. Eng. Comput.* **37** 760–9

Inoue H and Miyazaki A 1998 A noise reduction method for ECG signals using the dyadic wavelet transform *IEICE Trans. Fundam.* **vol E81A** 1001–7

Istepanian R S H, Hadjileontiadis L J and Panas S M 2001 ECG data compression using wavelets and higher order statistics *IEEE Trans. Inf. Technol. Biomed.* **5** 108–15

Istepanian R S H and Petrosian A A 2000 Optimal zonal wavelet-based ecg data compression for mobile telecardiology system *IEEE Trans. Inf. Technol. Biomed.* **4** 200–11

Ivanov P C, Amaral L A N, Goldberger A L, Havlin S, Rosenblum M G, Struzik Z R and Stanley H E 1999 Multifractality in human heartbeat dynamics *Nature* **399** 461–5

Ivanov P C, Rosenblum M G, Peng C-K, Mietus J, Havlin S, Stanley H E and Goldberger A L 1996 Scaling behaviour of heartbeat intervals obtained by wavelets-based time-series analysis *Nature* **383** 323–7

Jalaleddine S, Hutchens C, Strattan R and Coberly W 1990 ECG data compression techniques—a unified approach *IEEE Trans. Biomed. Eng.* **37** 329–43

Joho S, Asanoi H, Remah H A, Igawa A, Kameyama T, Nozawa T, Umeno K and Inoue H 1999 Time-varying spectral analysis of heart rate and left ventricular pressure variability during balloon coronary occlusion in humans *J. Am. Coll. Cardiol.* **34** 1924–31

Kadambe S, Murray R and Boudreaux-Bartels G F 1999 Wavelet transform-based QRS complex detector *IEEE Trans. Biomed. Eng.* **46** 838–48

Khadra L, Al-Fahoum A S and Al-Nashash H 1997 Detection of life-threatening cardiac arrhythmias using the wavelet transformation *Med. Biol. Eng. Comput.* **35** 626–32

Khalil M and Duchene J 2000 Uterine EMG analysis: a dynamic approach for change detection and classification *IEEE Trans. Biomed. Eng.* **47** 748–55

Köhler B U, Hennig C and Orglmeister R 2002 The principles of software QRS detection *IEEE Eng. Med. Biol.* **21** 42–57

Lee S-H, Zahouani H, Caterini R and Mathia T G 1998 Morphological characterisation of engineered surfaces by wavelet transform *Int. J. Mach. Tools Manuf.* **38** 581–9

Leman H and Marque C 2000 Rejection of the maternal electrocardiogram in the electrohysterogram signal *IEEE Trans. Biomed. Eng.* **47** 1010–7

Lemire D, Pharand C, Rajaonah J-C, Dube B and LeBlanc A R 2000 Wavelet time entropy, T wave morphology and myocardial ischemia *IEEE Trans. Biomed. Eng.* **47** 967–70

Lewandowski P, Meste O, Maniewski R, Mroczka T, Steinbach K and Rix H 2000 Risk evaluation of ventricular tachycardia using wavelet transform irregularity of the high-resolution electrocardiogram *Med. Biol. Eng. Comput.* **38** 666–73

Li C, Zheng C and Tai C 1995 Detection of ECG characteristic points using wavelet transforms *IEEE Trans. Biomed. Eng.* **42** 21–8

Link A, Endt P, Oeff M and Trahms L 2001 Variability of the QRS in high resolution electrocardiograms and magnetocardiograms *IEEE Trans. Biomed. Eng.* **48** 133–42

Lu Z, Kim D Y and Pearlman W A 2000 Wavelet compression of ECG signals by the set partitioning in hierarchical trees algorithm *IEEE Trans. Biomed. Eng.* **47** 849–55

Malik M 1996 Guidelines: heart rate variability *Eur. Heart J.* **17** 354–81

Mallat S G 1989 A theory for multiresolution signal decomposition: the wavelet representation *IEEE Trans. Pattern Anal. Mach. Intell.* **11** 674–93 chapter 3/chapter 7

Mallat S G 1998 *A Wavelet Tour of Signal Processing* (San Diego, CA: Academic)

Marrone A, Polosa A D, Scioscia G, Stramaglia S and Zenzola A 1999 Wavelet analysis of blood pressure waves in vasovagal syncope *Physica* A **271** 458–69

Martinez J P, Almeida R, Olmos S, Rocha A P and Laguna P 2004 A wavelet-based ECG delineator: evaluation on standard data bases *IEEE Trans. Biomed. Eng.* **51** 570–81

Meste O, Rix H, Casminal P and Thakor N V 1994 Ventricular late potentials characterization in time–frequency domain by means of a wavelet transform *IEEE Trans. Biomed. Eng.* **41** 625–34

Miaou S-G and Lin C-L 2002 A quality-on-demand algorithm for wavelet-based compression of electrocardiogram signals *IEEE Trans. Biomed. Eng.* **49** 233–9

Miaou S-G and Lin H-L 2000 Quality driven gold washing adaptive vector quantization and its application to ECG data compression *IEEE Trans. Biomed. Eng.* **47** 209–18

Miaou S-G, Yen H-L and Lin C-L 2002 Wavelet-based ECG compression using dynamic vector quantization with tree codevectors in single codebook *IEEE Trans. Biomed. Eng.* **49** 671–80

Morlet D, Peyrin F, Desseigne P, Touboul P and Rubel P 1993 Wavelet-analysis of high resolution signal averaged ECGs in postinfarction patients *J. Electrocardiol.* **26** 311–20

Nikoliaev N, Gotchev A, Egiazarian K and Nikolov Z 2001 Suppression of electromyogram interference on the electrocardiogram by transform domain denoising *Med. Biol. Eng. Comput.* **39** 649–55

Nyander A, Addison P S, Uchaipichat N, Watson J N and Newby D 2004 A wavelet transform-based frequency-specific entropy measure for the improved discrimination of HRV: application to the analysis of COPD patient HR during pollution experiments *CardioDigital Internal Report* 2004–1-HRV

Olmez T and Dokur Z 2003 Application of InP neural network to ECG beat classification *Neural Comput. Appl.* **11** 144–55

Park K L, Khil M J, Lee B C, Jeong K S, Lee K J and Yoon H R 2001 Design of a wavelet interpolation filter for enhancement of the ST-segment *Med. Biol. Eng. Comput.* **39** 1–6

Park K L, Lee K J and Yoon H R 1998 Application of a wavelet adaptive filter to minimise distortion of the ST-segment *Med. Biol. Eng. Comput.* **36** 581–6

Petrosian A, Prokhorov D, Homan R, Dasheiff R and Wunsch D 2000 Recurrent neural network based prediction of epileptic seizures in intra- and extracranial EEG *Neurocomputing* **30** 201–18

Pichot V, Bourin E, Roche F, Garet M, Gaspoz J-M, Duverney D, Antoniadis A, Lacour J-R and Barthelemy J-C 2002 Quantification of cumulated physical fatigue at the workplace *Plugers Arch.—Eur. J. Physiol.* **445** 267–72

Pichot V, Gaspoz J-M, Molliex S, Antoniadis A, Busso T, Roche F, Costes F, Quintin L, Lacour J-R and Barthelemy J-C 1999 Wavelet transform to quantify heart rate variability and to assess its instantaneous changes *J. Appl. Physiol.* **86** 1081–91

Popescu M, Cristea P and Bezerianos A 1999 Multiresolution distributed filtering: a novel technique that reduces the amount of data required in high resolution electrocardiography *Future Generation Comput. Syst.* **15** 195–209

Popescu M, Laskaris N, Chiladakis I, Stathopoulos C, Cristea P, Manolis A and Bezerianos A 1998 Beat-to-beat wavelet variance of the QRS complex as a marker of arrhythmogenic substrate in ventricular tachycardia patients *Physiol. Meas.* **19** 77–92

Rakotomamonjy A, Coast D and Marche P 1999 Wavelet-based enhancement of signal averaged electrocardiograms for late potential detection *Med. Biol. Eng. Comput.* **37** 750–9

Rakotomamonjy A, Migeon B and Marche P 1998 Automated neural network detection of wavelet preprocessed electrocardiogram potentials *Med. Biol. Eng. Comput.* **36** 346–50

Ramakrishnan A G and Saha S 1997 ECG coding by wavelet-based linear prediction *IEEE Trans. Biomed. Eng.* **44** 1253–61

Reed M J, Clegg G R and Robertson C E 2003 Analysing the ventricular fibrillation waveform *Resuscitation* **57** 11–20

Reed M J, Robertson C E and Addison P S 2005 Can heart rate variability measurements predict the onset of ventricular arrhythmias? *Q. J. Med.* **98** 87–95

Reinhardt L, Makijarvi M, Fetsch T, Montonen J, Sierra G, Martinez-Rubio A, Katila T, Borggrefe M and Breithardt G 1996 Predictive value of wavelet correlation functions of signal-averaged electrocardiograms in patients after anterior versus inferior myocardial infarction *J. Am. Coll. Cardiol.* **27** 53–9

Romero Legarreta I, Addison P S, Reed M J, Grubb N R, Clegg G R, Robertson C E and Watson J N 2005 Continuous wavelet transform modulus maxima analysis of the electrocardiogram: beat-to-beat characterisation and beat-to-beat measurement *Int. J. Wavelets, Multiresolution Inf. Process.* **3** 19–42

Rubel P, Hamidi S, Behlouli H, Couderc J-P, Fayn J, Forlini M-C, Maison-Blanche P, Miquel M, Coumel P and Touboul P 1996 Are serieal Holter QT, late potential and wavelet measurement clinically useful? *J. Electrocardiol.* **29** (Suppl.) 52–61

Sahambi J S, Tandon S M and Bhatt R K P 1997a Using wavelet transforms for ECG characterization: an on-line digital signal processing system *IEEE Eng. Med. Biol.* **16** 77–83

Sahambi J S, Tandon S M and Bhatt R K P 1997b Quantitative analysis of errors due to power-line interference and base-line drift in detection of onsets and offsets in ECG using wavelets *Med. Biol. Eng. Comput.* **35** 747–51

Sahambi J S, Tandon S M and Bhatt R K P 1998 Wavelet base ST-segment analysis *Med. Biol. Eng. Comput.* **36** 568–72

Sarkar T K and Su C 1998 A tutorial on wavelets from an electrical engineering perspective, part 2: the continuous case *IEEE Antennas Propag. Mag.* **40** 36–49

Senhadji L, Carrault G, Bellanger J J and Passariello G 1995 Comparing wavelet transforms for recognizing cardiac patterns *IEEE Trans. Med. Biol.* **13** 167–73

Shyu L-Y, Wu Y-H and Hu W 2004 Using wavelet transform and fuzzy neural network for VPC detection from the Holter ECG *IEEE Trans. Biomed. Eng.* **51** 1269–73

Sivannarayana N and Reddy D C 1999 Biorthogonal wavelet transforms for ECG parameters estimation *Med. Eng. Phys.* **21** 167–74

Sternickel K 2002 Automatic pattern recognition in ECG time series *Comput. Methods Prog. Biomed.* **68** 109–15

Stiles M K, Clifton D, Grubb N R, Watson J N and Addison P S 2004 Wavelet based analysis of heart rate dependent ECG features *Ann. Noninvasive Electrocardiol.* **9** 316–22

Strang G and Nguyen T 1996 *Wavelets and Filter Banks* (Wellesley: Wellesley-Cambridge)

Tan B-H, Shimizu H, Hiromoto K, Furukawa Y, Ohyanagi M and Iwasaki T 2003 Wavelet transform analysis of heart rate variability to assess the autonomic changes associated with spontaneous coronary spasm of variant angina *J. Electrocardiol.* **36** 117–24

Thakor N V, Sun Y-C, Rix H and Caminal P 1993a Multiwave: a wavelet-based ECG data compression algorithm *IEICE Trans. Inf. Syst.* **E76D** 1462–9

Thurner S, Feurstein M C, Lowen S B and Teich M C 1998a Receiver-operating-characteristic analysis reveals superiority of scale-dependent wavelet and spectral measures for assessing cardiac dysfunction *Phys. Rev. Lett.* **81** 5688–91

Thurner S, Feurstein M C and Teich M C 1998b Mulitresolution wavelet analysis of heartbeat intervals discriminates healthy patients from those with cardiac pathology *Phys. Rev. Lett.* **80** 1544–7

Tikkanen P E 1999 Nonlinear wavelet and wavelet packet denoising of electrocardiogram signal *Biol. Cybernetics* **80** 259–67

Toledo E, Gurevitz O, Hod H, Eldar M and Akselrod S 2003 Wavelet analysis of instantaneous heart rate: a study of autonomic control during thrombosis *Am. J. Physiol. Regul. Integr. Comp. Physiol.* **284** R1079–91

Tuteur F B 1989 Wavelet transforms in signal detection *Wavelets* ed J M Combs, A Grossmann and P Tchamitchian (Berlin: Springer) pp 132–8

Watson J N, Addison P S, Clegg G R, Holzer M, Sterz F and Robertson C E 2000 Evaluation of arrhythmic ECG signals using a novel wavelet transform method *Resuscitation* **43** 121–7

Watson J N, Addison P S, Clegg G R, Steen P A and Robertson C E 2005 Practical issues in the evaluation of methods for the prediction of shock outcome success in out-of-hospital cardiac arrest patients *Resuscitation* at press

Watson J N, Addison P S, Grubb N R, Clegg G R, Robertson C E and Fox K A A 2001 Wavelet-based filtering for the clinical evaluation of atrial fibrillation *23rd Annual Int. Conf. IEEE Engineering in Medicine and Biology Society (Istanbul, Turkey, 25–28 Oct.)*

Watson J N, Uchaipichat N, Addison P S, Clegg G R, Robertson C E, Eftestol T and Steen P A 2004 Improved prediction of defibrillation success for out-of-hospital VF cardiac arrest using wavelet transform methods *Resuscitation* **63** 269–75

Wiklund U, Akay M and Niklasson U 1997 Short-term analysis of heart-rate variability by adapted wavelet transforms *IEEE Eng. Med. Biol.* **16** 113–8

Williams J R and Amaratunga K 1994 An introduction to wavelets in engineering *Int. J. Numer. Methods Eng.* **37** 2365–88

Wu S, Qian Y, Gao Z and Lin J 2001 A novel method for beat-to-beat detection of ventricular late potentials *IEEE Trans. Biomed. Eng.* **48** 931–5

Yi G, Hnatkova K, Mahon N G, Keeling P J, Reardon M, Camm A J and Malik M 2000 Predictive value of wavelet decomposition of the signal averaged electrocardiogram in idiopathic dilated cardiomyopathy *Eur. Heart J.* **21** 1015–22

Zhang X-S, Zhu Y-S, Thakor N V, Wang Z-M and Wang Z-Z 1999 Modeling the relationship between concurrent epicardial action potentials and bipolar electrograms *IEEE Trans. Biomed. Eng.* **46** 365–76

Zhang X-S, Zhu Y-S and Zhang X-J 1997 New approach to studies on ECG dynamics: extraction and analyses of QRS complex irregularity time series *Med. Biol. Eng. Comput.* **35** 467–74